QUANTUM CONTROL OF HYPERBOLIC METAMATERIALS

by

Onur Danacı

A Thesis Submitted to the
Graduate School of Sciences and Engineering
in Partial Fulfillment of the Requirements for
the Degree of

Master of Science

in

Physics

Koç University

January, 2015

Koç University

Graduate School of Sciences and Engineering

This is to certify that I have examined this copy of a master's thesis by

Onur Danacı

and have found that it is complete and satisfactory in all respects,
and that any and all revisions required by the final
examining committee have been made.

Committee Members:

Prof. Özgür Esat Müstecaplıoğlu (Supervisor)

Assoc. Prof. Kaan Güven

Assist. Prof. Şükrü Ekin Kocabaş

Date:

ABSTRACT

In this thesis, we study atom-photon interactions on quantum level, inside Hyperbolic Metamaterials (HMM). First, the macroscopic Maxwell equations are examined in the light of Green's dyadics. Second, this formalism, combined with Drude-Lorentz model of materials, is used to infer the existence of *Surface Plasmon Polariton* excitations and hyperbolic dispersion in layered HMM by means of *Effective Medium Approximation*. Third, many-body polaritonic Hamiltonian is diagonalized, and, the medium assisted field is found to be dependent on classical Green's tensor, while no reference to microscopic model is needed. Last, as a test case, QED in complex media based on classical Green's tensor formalism is used to calculate single photon excitation probability for an atom embedded in l-HMM system (Ag/$Ti0_2$ layers), when it is shed by a time-inverted, conical, single photon pulse. High excitation probabilities are found, yet problem of outcoupling leaves the implementation impractical.

ÖZETÇE

Bu tezde, Hiperbolik Metamateryal (HMM) içerisine gömülü atomların fotonlarla kuantum mertebesindeki etkileşimlerini inceliyoruz. lk olarak, makroskopik Maxwell denklemleri diyadik Green fonksiyonları ışığında gözden geçirildi. kinci olarak, bu formalizm, Drude-Lorentz metal elektron kuramıyla birlikte düşünüldüğünde Yüzey Plazmon Polariton uyarımlarının ve katmanlı HMM'lerdeki (l-HMM) hiperbolik dispersiyonun varlığını çıkarsamak amacıyla Efektif Ortam Yaklaştırımı'na binaen kullanıldı. üçüncü olarak, çoklu cisim polariton Hamiltonyanı köşegenleştirildi. Ayrıca, ortam destekli elektromanyetik alanın, herhangi bir mikroskopik modele dayanmaksızın yalnızca klasik Green tensörüne bağlı olduğu bulundu. Son ve deneme amaçlı olarak, klasik Green tensörü formalizmine binaen, karmaşık ortamlarda kuantum elektrodinamik kuramını l-HMM ortamına ($Ag/Ti0_2$ katmanları) gömülü bir atomun tekil foton uyarım olasılığını hesaplamak için kullanıyoruz. Bu amaçla, atomumuzun zamanda geriye döndürülmüş, konik bir tekil foton sinyaliyle aydınlatıldığını varsayıyoruz. Yüksek uyarım olasılıkları öngörsek de, sistemin dış dünyayla etkileşim noksanlığı, uygulamaları işlevsiz kılmakta.

ACKNOWLEDGMENTS

I want to thank Prof. Özgür Esat Müstecaplıoğlu for showing me why a researcher should focus on numerical values of physical parameters of system in question instead of getting drowned in complex mathematics in the field of Quantum Optics, and, not forsaking me. I want to thank Nader Ghazanfari for the cheerful physics discussions and the most delicious rice he cooked. Last, but not least, I want to thank Assist. Prof. Şükrü Ekin Kocabaş and Gül Seda Ünal for their help on Green's tensors.

Dedicated to the fading hopes of recovery from pathological levels of academic competition culture that reached the verge of cannibalism. No material gain is worth the corrosion of character. If cannibalism is tolerated even once for the seemingly legitimate causes, future of the humankind will be doomed. Solidarity forever.

TABLE OF CONTENTS

Chapter 1

INTRODUCTION

Almost 15 decades past since the theory of Maxwell equations, 9 decades since Quantum mechanics, 7 decades since Quantum Electrodynamics and 5 decades since Quantum Optics were well established, yet new phenomena and innovations still keep emerging. It can partly be attributed to the wide scope of related phenomena and applications leading to almost infinite amount of possibilities, partly to well known yet not feasible prospects enabled by contemporary techniques and devices, and partly to losses in history and communication; still many treasures have been waiting to be unearthed in Soviet or pre-war German scientific journals.

Implementations of quantum information science [1] [2] and quantum imaging [3] [4] [5] are one set of novelties facilitated by new laser and solid state technologies, and, excellence in experimental control. Phenomena related to Surface Plasmon Resonance is observed in the beginning of 20th century [6], and the theoretical framework is devised by Wood and Lord Rayleigh [7] [8] , but the scientific and industrial focus had to wait '60s fabrication, spectroscopy techniques and invention of laser, but it had not peaked until metamaterial [9] "revolution" of 21st century. Classical framework of subdiffraction imaging and near-field optics, such as angular spectrum representation, already devised by Sommerfeld [10], Zenneck [11] and Weyl [12], and, quantum theory of the complex electromagnetic media devised by Fano [13] and Hopfield [14], nevertheless they have never been as significant until the invention of scanning optical microscope and emergence of quantum plasmonics [15] [16] [17] [18] [19] [20] [21] [22] [23].

Since Pendry [24] predicted the possibility of left-handed materials (negative refraction), metamaterials are on focus. They have promising features like cloaking [25] and subdiffraction imaging [26].

One of the children of metamaterial "revolution" is layered Hyperbolic Metamaterials (l-HMM) [27] [28] [29] . These artificial materials are extremely anisotropic because they both have metallic and dielectric characteristics. The hyperbolic dispersion relation, as a product of extreme anisotropy, enables generation and transfer of high-k states [30], thus it is offered as a candidate of hyperlens [31] for subdiffraction imaging. Due to spontaneous emission rate increase [32] [33] and directionality [34] inside l-HMM, it is also proposed as a single photon source, a platform of quantum optics and information.

In this thesis, we want to establish a theoretical formalism to examine atom-photon interactions inside HMMs on quantum level. We want to unleash HMMs potential as a quantum metamaterial [35] [15], and use it as a platform of quantum information and imaging. Therefore, in the first chapter, we start by classical foundations of Hyperbolic Metamaterials. In the second chapter, we develop the theory of atoms interacting with medium-assisted quantum field in complex media. In the last chapter, we apply this theory to the problem of single photon excitation of an atom embedded in HMM.

Chapter 2

PLASMONICS AND HYPERBOLIC METAMATERIALS

2.1 Macroscopic Maxwell Equations

Many sources on optics [36] [37] [38] start with the discussion of macroscopic Maxwell equations. Without giving a reference to any microscopical model, we can give differential form of these equations as follows,

$$\begin{aligned} \nabla \cdot \mathbf{D}(\mathbf{r},t) &= \rho_{ext}(\mathbf{r},t) \\ \nabla \cdot \mathbf{B}(\mathbf{r},t) &= 0 \\ \nabla \times \mathbf{E}(\mathbf{r},t) &= -\frac{\partial \mathbf{B}(\mathbf{r},t)}{\partial t} \\ \nabla \times \mathbf{H}(\mathbf{r},t) &= \mathbf{j}(\mathbf{r},t) + \frac{\partial \mathbf{D}(\mathbf{r},t)}{\partial t} \end{aligned} \tag{2.1}$$

Electric displacement term in fourth equation, $\mathbf{D}(\mathbf{r},t)$, is related to macroscopic electric field, $\mathbf{E}(\mathbf{r},t)$, through overall polarization of the media, $\mathbf{P}(\mathbf{r},t)$, same applies for magnetic field and magnetization,

$$\mathbf{D}(\mathbf{r},t) = \varepsilon_0 \mathbf{E}(\mathbf{r},t) + \mathbf{P}(\mathbf{r},t) \tag{2.2}$$

$$\mathbf{B}(\mathbf{r},t) = \mu_0 \mathbf{H}(\mathbf{r},t) \tag{2.3}$$

Once we assume isotropic, linear and local response from the media, we get the expression below in accordance with fluctuation-dissipation theorem [39] , where we define linear response function, χ, known as electric susceptibility,

$$\mathbf{P}(\mathbf{r},t) = \int_t^\infty dt' \chi(\mathbf{r},t-t') \mathbf{E}(\mathbf{r},t') \tag{2.4}$$

Defining dielectric function in frequency domain, $\varepsilon(\mathbf{r},\omega)$, using convolution theorem to gather all (delayed) responses in time domain, t, t', $t-t'$, and combining with equations above, we get,

$$\varepsilon(\mathbf{r},\omega) = 1 + \int_t^{\infty} dt' e^{i\omega(t-t')}\chi(\mathbf{r},t') \tag{2.5}$$

$$\mathbf{D}(\mathbf{r},\omega) = \varepsilon(\mathbf{r},\omega)\mathbf{E}(\mathbf{r},\omega) \tag{2.6}$$

By using Kramers-Krönig relations [40], we could separate real (related to dispersion) and imaginary (related to absorption) parts of the dielectric function in frequency domain, which are related to each other,

$$\varepsilon'(\mathbf{r},\omega) = 1 - \frac{1}{\pi}\wp\int d\omega' \frac{\varepsilon''(\mathbf{r},\omega')}{\omega-\omega'} \tag{2.7}$$

$$\varepsilon''(\mathbf{r},\omega) = \frac{1}{\pi}\wp\int d\omega' \frac{\varepsilon'(\mathbf{r},\omega')-1}{\omega-\omega'} \tag{2.8}$$

If we take Fourier transforms of Maxwell equations with respect to time domain, such that time derivatives, $\frac{\partial}{\partial t}$, bring frequency term, $-i\omega$, on the exponent to front, we get,

$$\boldsymbol{\nabla}\cdot\varepsilon(\mathbf{r},\omega)\mathbf{E}(\mathbf{r},\omega) = \rho(\mathbf{r},\omega) \tag{2.9}$$

$$\boldsymbol{\nabla}\cdot\varepsilon(\mathbf{r},\omega)\mathbf{B}(\mathbf{r},\omega) = 0 \tag{2.10}$$

$$\boldsymbol{\nabla}\times\mathbf{E}(\mathbf{r},\omega) = i\omega\mathbf{B}(\mathbf{r},\omega) \tag{2.11}$$

$$\boldsymbol{\nabla}\times\mathbf{B}(\mathbf{r},\omega) = \mu_0\mathbf{j}(\mathbf{r},\omega) - i\frac{\omega^2}{c^2}\mathbf{B}(\mathbf{r},\omega) \tag{2.12}$$

$$\tag{2.13}$$

Once we bring these equations altogether, we get a nonhomogeneous wave equation with respect to current density as a source term.

$$(\frac{\omega^2}{c^2} - \boldsymbol{\nabla}\times\boldsymbol{\nabla}\times)\mathbf{E}(\mathbf{r},\omega) = -i\omega\mu_0\mathbf{j}(\mathbf{r},\omega) \tag{2.14}$$

This can be solved for homogeneous case, then the problem of non homogeneity is reduced to find the map, which is a **Green's Dyad** (or a tensor), from sources, $\mathbf{j}(\mathbf{r}', \omega)$, situated in source coordinates, $\mathbf{r}'$, to target field, $\mathbf{E}(\mathbf{r}, \omega)$, on, target position, $\mathbf{r}$. A Green's function, or a tensor as a three dimensional map, needs to solve this equation for the homogeneous case, leaving only identity tensor (matrix) and a Dirac delta function in between source and target coordinates on right hand side,

$$(\boldsymbol{\nabla} \times \boldsymbol{\nabla} \times -\frac{\omega^2}{c^2}\varepsilon(\mathbf{r}, \omega))\mathbf{G}(\mathbf{r}, \mathbf{r}', \omega) = \mathbf{I}\delta(\mathbf{r} - \mathbf{r}') \tag{2.15}$$

If we multiply both sides with some constants and current densities in source coordinates, $\mathbf{j}(\mathbf{r}', \omega)$, and take the integral for the volume of the body containing the sources we get,

$$\mathbf{E}(\mathbf{r}, \omega) = i\omega\mu_0 \int d^3\mathbf{r}'\mathbf{G}(\mathbf{r}, \mathbf{r}', \omega)\mathbf{j}(\mathbf{r}', \omega) \tag{2.16}$$

This integral maps the electric field generated by each current in source volume to target coordinate, then superimpose them.

2.2 Drude-Lorentz Model of Dielectrics and Metals

The optical response of dielectric media is positive, real and almost lossless, because the electrons are tightly bounded to nuclei of the respective atoms. The metals, on the other hand, have a negative and lossy response to electromagnetic radiation, which can be accounted by a gas of electrons roaming freely with respect to ion cores and colliding to each other; more or less a plasma model when interband transitions are not considered -not negligible for noble metals. The Drude-Lorentz model (classical) starts with freely oscillating charges that can be easily driven with electric fields, and possess phenomenological collision(damping) rates, $gamma = 1/\tau$ and optical masses, m associated to them. Typical relaxation time [36] of the free electron gas is around $\tau = 10^{-14}$s or $\gamma = 100$ THz. When an external electrical field $\mathbf{E}$ is applied, an electron's equation of motion is

$$m\ddot{\mathbf{x}} + m\gamma\dot{\mathbf{x}} = -e\mathbf{E} \tag{2.17}$$

When $\mathbf{E}(t) = \mathbf{E}_0 e^{-i\omega t}$ and $\mathbf{x}(t) = \mathbf{x}_0 e^{-i\omega t}$ time dependences are incorporated:

$$\mathbf{x}(t) = \frac{e}{m(\omega^2 + i\gamma\omega)}\mathbf{E}(t) \tag{2.18}$$

Since the dipole moment is $\mathbf{p} = -e\mathbf{x}$ and the macroscopic polarization is the overall dipole moments of all particles averaged over the whole volume $\mathbf{P} = (N/V)\mathbf{p} = -ne\mathbf{x}$

$$\mathbf{P} = -\frac{ne^2}{m(\omega^2 + i\gamma\omega)}\mathbf{E}(t) \tag{2.19}$$

By defining plasma frequency, $\omega_p = \sqrt{\frac{ne^2}{\varepsilon_0 m}}$ and making use of the definition of electric displacement $\mathbf{D} = \varepsilon_0\varepsilon(\omega)\mathbf{E}$ we get the expression for the dielectric function of free electron gas, and its real and imaginary constituents

$$\mathbf{D} = \varepsilon_0(1 - \frac{w_p^2}{m(\omega^2 + i\gamma\omega)})\mathbf{E}(t) \tag{2.20}$$

$$\varepsilon(\omega) = 1 - \frac{\omega_p^2}{\omega^2 + i\gamma\omega} \tag{2.21}$$

$$\varepsilon_R(\omega) = 1 - \frac{\omega_p^2\tau^2}{1 + \omega^2\tau^2} \tag{2.22}$$

$$\varepsilon_I(\omega) = \frac{\omega_p^2\tau}{\omega(1 + \omega^2\tau^2)} \tag{2.23}$$

In the frequency domain $\omega < \omega_p$ metals have dielectric functions whose real part is negative, $\varepsilon_R < 0$, and imaginary part really small $\varepsilon_I \approx 0$. They are mostly reflective to incoming light and the fields emanating from metals in this region can propagate only short distances due to decay. In the $\omega > \omega_p$ domain, on the other hand, most light is transmitted through.

In the case of noble metals, Drude-Lorentz model can not account for high-frequency response. This can be overcome by adding the residual polarization from ion cores, $\mathbf{P}_\infty =$

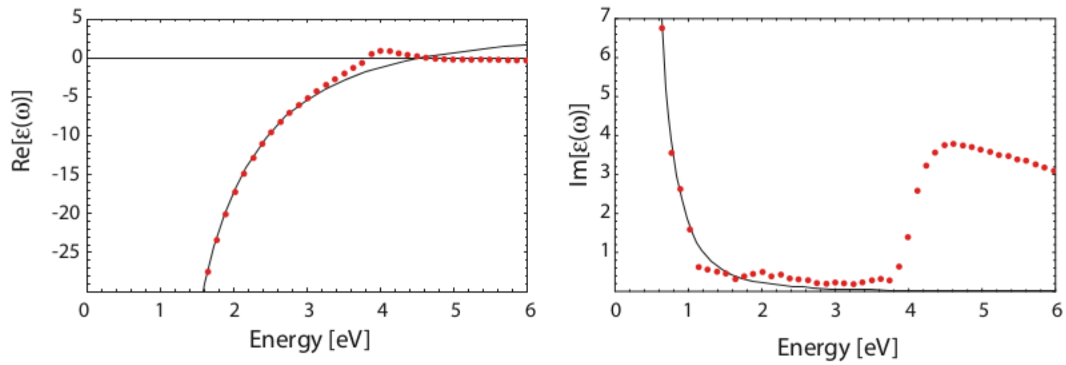

Figure 2.1: Real and Imaginary parts of silver's dielectric response, $\varepsilon(\omega)$, from Johnson and Christy's(1972)data [41]. Red dots are the data and the curves are fitted to Drude-Lorentz model(adapted from Maier [36])

$\varepsilon_0 (\varepsilon_\infty - 1)$,

$$\varepsilon(\omega) = \epsilon_\infty - \frac{\omega_p^2}{\omega^2 + i\gamma\omega} \tag{2.24}$$

$$\tag{2.25}$$

and taking interband transitions into account.

$$m\ddot{\mathbf{x}} + m\gamma\dot{\mathbf{x}} + m\omega_0^2\mathbf{x} = -e\mathbf{E} \tag{2.26}$$

Interband transitions lead to another classical oscillator term, a bound electron with resonance frequency ω_0 . Because of this term, Lorentz-oscillator terms, $\frac{A_i}{\omega_i^2 - \omega^2 - i\gamma_i\omega}$ must be added to the solution. [36] [42]. Let $\tilde{n}$ be bound electron density and $\tilde{\omega}_p = \sqrt{\frac{\tilde{n}e^2}{m\varepsilon_0}}$,

$$\varepsilon_{\text{Interband}} = 1 + \frac{\tilde{\omega}_p^2}{(\omega_0^2 - \omega^2) - i\gamma\omega} \tag{2.27}$$

2.3 Surface Plasmon Polaritons and Electromagnetic Response of Layered Media

2.3.1 Surface Plasmon Resonance

Presence of plasma oscillations inside metals, as we saw in the last chapter, cause peculiar optical phenomena. It makes [36] metals highly reflective in frequencies below bulk plasmon frequency, ω_p, by making real part of relative permittivity negative, $\varepsilon_R < 0$. Also, it makes metals lossy because of the many damping channels of these bulk plasmons make imaginary part of permittivity positive, $\varepsilon_I > 0$. When such a metal is combined with a dielectric material possessing positive permittivity in real part, $\varepsilon_R > 0$, even in the simplest configuration such as two layer stack, field is focused and forming hotspots on the boundary.

Figure 2.2: Surface plasma resonance at metal dielectric boundary, Adapted from Maier [36]

Starting point [36] is the electromagnetic wave equation in the absence of external charge and currents.

$$\nabla \times \nabla \times \mathbf{E} = -\mu_0 \frac{\partial^2 \mathbf{D}(\mathbf{r}, t)}{\partial t^2} \tag{2.28}$$

Once harmonic time dependence, $\mathbf{E}(\mathbf{r}, t) = \mathbf{E}(\mathbf{r})e^{-i\omega t}$, is assumed, well known Helmholtz equation is recovered,

$$\nabla^2 \mathbf{E} + \frac{\omega^2}{c^2} \varepsilon \mathbf{E} = 0 \tag{2.29}$$

This equation has two solutions for two different polarizations for our configuration, *Transverse Electric* (TE) or s polarization, and, *Transverse Magnetic* (TM) or p polarization. Both solutions keep fields non zero in the vicinity of boundary and letting them decay everywhere else. Hence, in addition to broken symmetry of the system due to layer stack (spherical symmetry is replaced by azimuthal or cylindrical symmetry), presence of metal-dielectric boundary effectively makes system anisotropic as we will see in later sections. The case of TM polarization yield even more strange phenomena. The fields above, $z > 0$, and, below, $z < 0$, the boundary are as follows,

$$H_y(z) = A^{diel,metal} e^{i\beta x} e^{\mp k_z^{diel,metal}} \tag{2.30}$$

$$E_x(z) = \pm i A^{diel,metal} \frac{1}{\omega\varepsilon_0\varepsilon_{diel,metal}} k_z^{diel,metal} e^{i\beta x} e^{\mp k_z^{diel,metal}} \tag{2.31}$$

$$E_z(z) = -A^{metal} \frac{\beta}{\omega\varepsilon_0\varepsilon_{diel,metal}} e^{i\beta x} e^{\mp k_z^{diel,metal}} \tag{2.32}$$

And, for $\alpha_i = \sqrt{\varepsilon_i \frac{\omega^2}{c^2} - k_\rho^2}$, Fresnel reflection coefficient [38] for TM polarization is,

$$R_{i,i-1}^{TM} = \frac{\varepsilon_{i-1}\alpha_i - \varepsilon_i\alpha_{i-1}}{\varepsilon_{i-1}\alpha_i + \varepsilon_i\alpha_{i-1}} \tag{2.33}$$

The continuity boundary condition for H_y and $\varepsilon_i E_z$, which also corresponds to the case [38] where Fresnel reflection coefficient, R^{TM}, equals to 0, yielding,

$$A^{metal} = A^{diel} \tag{2.34}$$

$$\frac{k_z^{diel}}{k_z^{metal}} = -\frac{\varepsilon_{diel}}{\varepsilon_{metal}} \tag{2.35}$$

From this, the presence of propagating surface modes, known as *Surface Plasmon Polaritons* (SPP) can be inferred. SPPs have the following dispersion relations, also shown in Figure 2.3,

$$c^2 (k_{SP})^2 = c^2\beta^2 = \left(\frac{\omega}{c}\right)^2 \frac{\varepsilon_{diel}\varepsilon_{metal}}{\varepsilon_{diel} + \varepsilon_{metal}} \tag{2.36}$$

$$\left(k_z^{diel,metal}\right)^2 = \varepsilon_{diel,metal} \left(\frac{\omega}{c}\right)^2 - k_{SP}^2 \tag{2.37}$$

Since k_x^2 is greater than, $\varepsilon_{diel,metal} \left(\frac{\omega}{c}\right)^2$, k_z is imaginary, hence the wave becomes evanescent once it is away from the interface. SPPs propagate horizontally along the interface, by wave vector k_x.

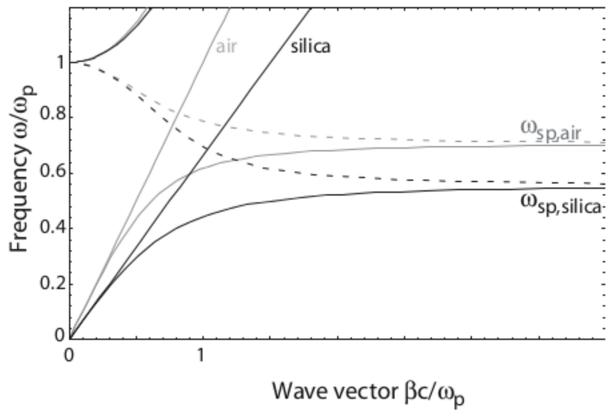

Figure 2.3: Dispersion relations for SPP at air silica interface, Adapted from Maier [36]

2.4 Layered Hyperbolic Metamaterials

The system we are going to examine is an artificial material, made out of metal-dielectric layers [35]. As already anticipated in last section, excitation of SPPs in metal-dielectric interfaces lead to strong anisotropy that can not be found in nature, making the metamaterial behave metalic in one direction and dielectric in other [30]. Once material parameters are engineered correctly, an odd type of uniaxial metamaterial with hyperbolic dispersion relations, known as layered Hyperbolic Metamaterial (l-HMM) can be fabricated. We will, first, examine field distribution of such a multilayer system. Then, utilizing effective medium approximation [43], we formulate anisotropy and hyperbolicity of these systems, and, use Green's dyad [42] in this frame to calculate Purcell effect [44] and electric field profile [45].

2.4.1 Green's Tensor for Multilayer Dielectrics

Novotny [42] starts the calculation of Green's dyad associated to an electric dipole (atom), sitting on or embedded in multilayer dielectric (or metal) media by Helmholtz equation for vector potential in Lorentz gauge,

$$\left[\boldsymbol{\nabla}^2 + k^2\right] \mathbf{A}(\mathbf{r}) = -\mu\mu_0 \mathbf{j}(\mathbf{r}) \tag{2.38}$$

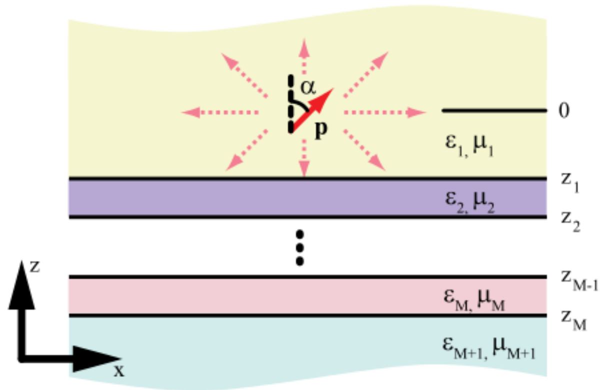

Figure 2.4: Electric dipole embedded or positioned above dielectric stack, Adapted from [43]

Then, scalar Green's function can be obtained for this equation,

$$\left[\boldsymbol{\nabla}^2 + k^2\right] G_0(\mathbf{r}, \mathbf{r}') = -\delta(\mathbf{r} - \mathbf{r}') \tag{2.39}$$

Only solution for scalar Green's function [46] [47] in free-space is the spherical wave,

$$G_0(\mathbf{r}, \mathbf{r}') = \frac{e^{i \pm k|\mathbf{r}-\mathbf{r}'|}}{4\pi|\mathbf{r} - \mathbf{r}'|} \tag{2.40}$$

Since ,an electric dipole (atom), $\mathbf{p}$, is the source of electromagnetic fields in this problem, current density and vector potential are given as,

$$\mathbf{j}(\mathbf{r}) = -i\omega\delta(\mathbf{r} - \mathbf{r}')\mathbf{p} \tag{2.41}$$

$$\mathbf{A}(\mathbf{r}) = \mu_0\mu \int d^3r'\mathbf{j}(\mathbf{r}')G_0(\mathbf{r}, \mathbf{r}') = \mathbf{p}\frac{k_1^2}{i\omega\epsilon_0\epsilon_1}G_0(\mathbf{r}, \mathbf{r}') \tag{2.42}$$

Using the Weyl identity [12], vector potential can be written in the form of angular spectrum representation,

$$\mathbf{A}(\mathbf{r}) = \mathbf{p}\frac{k_1^2}{8\pi^2\omega\epsilon_0\epsilon_1} \iint_{-\infty}^{\infty} \frac{1}{k_1} e^{i[k_x(x-x_0)+k_y(y-y_0)+k_{z_1}|z-z_0|]} \tag{2.43}$$

Using the identity, $\mathbf{E} = i\omega\left[1 + k_1^{-2}\boldsymbol{\nabla}\boldsymbol{\nabla}\cdot\right]\mathbf{A}$, we get the general form of Green's tensor,

$$\mathbf{G}(\mathbf{r},\mathbf{r}_0) = \frac{i}{8\pi^2}\iint_{-\infty}^{\infty} \mathbf{M} e^{i[k_x(x-x_0)+k_y(y-y_0)+k_{z_1}|z-z_0|]} \tag{2.44}$$

$$\mathbf{M} = \frac{1}{k_1^2 k_{z_1}} \begin{bmatrix} k_1^2 - k_x^2 & -k_x k_y & \mp k_x k_{z_1} \\ -k_x k_y & k_1^2 - k_y^2 & \mp k_y k_{z_1} \\ \mp k_x k_{z_1} & \mp k_y k_{z_1} & k_1^2 - k_{z_1}^2 \end{bmatrix} \tag{2.45}$$

To be able to apply Fresnel transmission and reflection coefficients, Green's dyad should be separated into parts corresponding TE and TM polarizations. Using radial part of wavevector in cylindrical coordinates, $k_\rho^2 = k_x^2 + k_y^2$,

$$\mathbf{M} = \mathbf{M}^{TE} + \mathbf{M}^{TM} \tag{2.46}$$

$$\mathbf{M}^{TE} = \frac{1}{k_\rho^2 k_{z_1}} \begin{bmatrix} k_y^2 & -k_x k_y & 0 \\ -k_x k_y & k_x^2 & 0 \\ 0 & 0 & 0 \end{bmatrix} \tag{2.47}$$

$$\mathbf{M}_{\mp}^{TM} = \frac{1}{k^2 k_\rho^2} \begin{bmatrix} k_x^2 k_z & k_x k_y k_z & \mp k_x k_\rho^2 \\ k_x k_y k_z & k_y^2 k_z & \mp k_y k_\rho^2 \\ \mp k_x k_\rho^2 & \mp k_y k_\rho^2 & k_\rho^4 / k_z \end{bmatrix} \tag{2.48}$$

In the second matrix above, $\mathbf{M}_{\mp}^{TM}$, "-" corresponds to upper half-space, vice versa. Matrices related to reflection and transmission Green's tensors, are calculated using matrices for different polarizations and generalized Fresnel coefficients associated to these polarizations,

$$\mathbf{M}_r^{TE} = r^{TE}(k_x, k_y)\mathbf{M}^{TE} \tag{2.49}$$

$$\mathbf{M}_r^{TM} = -r^{TM}(k_x, k_y)\mathbf{M}_{-}^{TM} \tag{2.50}$$

$$\mathbf{M}_t^{TE} = t^{TE}(k_x, k_y)\mathbf{M}^{TE} \tag{2.51}$$

$$\mathbf{M}_t^{TM} = \frac{t^{TM}(k_x, k_y)}{k_1 k_n k_\rho^2} \begin{bmatrix} k_x^2 k_{z_n} & k_x k_y k_{z_n} & k_x k_\rho^2 k_{z_n}/k_{z_1} \\ k_x k_y k_{z_n} & k_y^2 k_{z_n} & k_y k_\rho^2 k_{z_n}/k_{z_1} \\ k_x k_\rho^2 & k_y k_\rho^2 & k_\rho^4 / k_z \end{bmatrix} \tag{2.52}$$

Where generalized reflection and transmission coefficients, $r^{TE,TM}$, $t^{TE,TM}$, are calculated by Fresnel coefficients, and phase terms using geometric series, depending on the multilayer geometry and material parameters. Generalized reflection and transmission coefficient for the boundary between regions i and $i-1$ is given [38] as,

$$r_{i,i-1}^{TM,TE} = \frac{R_{i,i-1}^{TM,TE} + R_{i-1,i-2}^{TM,TE} e^{i2\beta_{i-1}(d_{i-1}-d_{i-2})}}{1 + R_{i,i-1}^{TM,TE} R_{i-1,i-2}^{TM,TE} e^{i2\beta_{i-1}(d_{i-1}-d_{i-2})}} \tag{2.53}$$

$$t_{i,i-1}^{TM,TE} = \frac{T_{i,i-1}^{TM,TE}}{1 + R_{i,i-1}^{TM,TE} R_{i-1,i-2}^{TM,TE} e^{i2\beta_{i-1}(d_{i-1}-d_{i-2})}} \tag{2.54}$$

$$R_{i,i-1}^{TE} = \frac{\alpha_i - \alpha_{i-1}}{\alpha_i + \alpha_{i-1}} \tag{2.55}$$

$$T_{i,i-1}^{TM} = \frac{2\varepsilon_i \alpha_{i-1}}{\varepsilon_{i-1}\alpha_i + \varepsilon_i \alpha_{i-1}} \tag{2.56}$$

$$T_{i,i-1}^{TE} = \frac{2\alpha_i}{\alpha_i + \alpha_{i-1}} \tag{2.57}$$

As a result, reflection and transmission Green's tensors are given as follows,

$$\mathbf{G}_{ref}(\mathbf{r},\mathbf{r}_0) = \frac{i}{8\pi^2} \iint_{-\infty}^{\infty} (\mathbf{M}_r^{TE} + \mathbf{M}_r^{TM}) e^{i[k_x(x-x_0)+k_y(y-y_0)+k_{z_1}(z+z_0)]} \tag{2.58}$$

$$\mathbf{G}_{tr}(\mathbf{r},\mathbf{r}_0) = \frac{i}{8\pi^2} \iint_{-\infty}^{\infty} (\mathbf{M}_t^{TE} + \mathbf{M}_t^{TM}) e^{i[k_x(x-x_0)+k_y(y-y_0)-k_{z_n}(z+\lambda)+k_{z_1}z_0]} \tag{2.59}$$

2.4.2 Effective Medium Approximation for Layered Medium

The widespread method to obtain effective dielectric response from a composite, complex medium is to take spatial averages of the fields in the mesoscopic scale over materials. Typical example is Maxwell-Garnett geometry [48] [43] , where a lattice of atoms, or roughly dielectric spherical inclusions, are hosted inside another dielectric medium. The macroscopic field is not enough for polarizability, hence effective dielectric response, calculations, local field corrections from neighbouring dipoles are required.

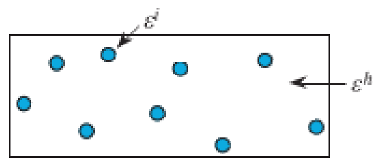

Figure 2.5: Maxwell-Garnett Topology (adapted from Shalaev [43])

$$\mathbf{p} = \alpha \left(\mathbf{E}_{macro} + \text{local field corrections}\right) \tag{2.60}$$

$$\int dV \mathbf{E}_{micro} = -\frac{4\pi}{3}\mathbf{p} \tag{2.61}$$

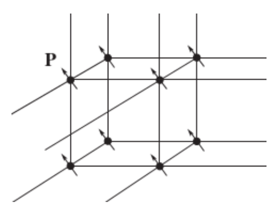

Figure 2.6: Lattice of Dipoles (adapted from [43]

For the lattice of N atoms inside the volume V, the local field correction is

$$\mathbf{p} = \alpha \left[\mathbf{E} - \frac{-\frac{4\pi}{3}\mathbf{p}}{V/N}\right] \tag{2.62}$$

$$\mathbf{P} = \frac{N}{V}\mathbf{p} = \frac{N}{V}\alpha\left(\mathbf{E} + \frac{4\pi}{3}\mathbf{P}\right) \tag{2.63}$$

Using the definition of the electric displacement, $\mathbf{D} = \mathbf{E} + 4\pi\mathbf{P} = \epsilon\mathbf{E}$, famous Clausius-Mossotti equation is obtained

$$\frac{\epsilon - 1}{\epsilon + 2} = \frac{4\pi}{3}\frac{N}{V}\alpha \tag{2.64}$$

In the case of Maxwell-Garnett topology, where we include dielectric properties of the host medium, electric field of spherical inclusions of $r = a$ are not equal to overall field due to depolarization field. Effective polarizability is calculated by

$$\mathbf{P}_{inc} = \frac{\epsilon_{inc} - 1}{4\pi}\mathbf{E}_{inc} = \frac{3}{4\pi}\frac{\epsilon_{inc} - \epsilon_{host}}{\epsilon_{inc} + 2\epsilon_{host}}\mathbf{E}_0 \tag{2.65}$$

$$\mathbf{p}_{inc} = \frac{4\pi}{3}a^3\mathbf{P}_{inc} = a^3\frac{\epsilon_{inc} - \epsilon_{host}}{\epsilon_{inc} + 2\epsilon_{host}}\mathbf{E}_0 \tag{2.66}$$

$$\alpha = a^3\frac{\epsilon_{inc} - \epsilon_{host}}{\epsilon_{inc} + 2\epsilon_{host}} \tag{2.67}$$

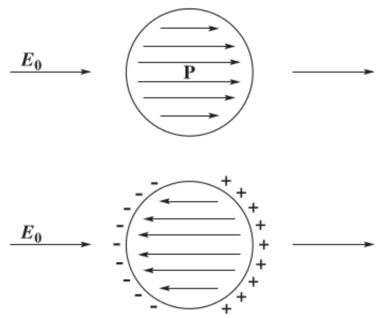

Figure 2.7: Depolarization field of inclusion sphere in a host dielectric (adapted from Shalaev [43])

Combining this expression with Clausius-Mossotti equation by noticing dielectric inclusions are not suspended in vacuum but host medium, one could obtain effective dielecric constant by averaging over the whole volume. The effective dielectric constant obtained is closely associated with filling factor, f, which is related to ratio of different dielectric media and geometry.

$$\frac{\epsilon_{eff} - \epsilon_{host}}{\epsilon_{eff} + 2\epsilon_{host}} = \frac{4\pi}{3}\frac{N}{V}\left(a^3\frac{\epsilon_{inc} - \epsilon_{host}}{\epsilon_{inc} + 2\epsilon_{host}}\right)\} = f\frac{\epsilon_{inc} - \epsilon_{host}}{\epsilon_{inc} + 2\epsilon_{host}} \tag{2.68}$$

If there are two dielectric inclusions, ϵ_1 and ϵ_2, of filling factors, f_1 and f_2, inside the host medium, the expression changes into

$$\frac{\epsilon_{eff} - \epsilon_{host}}{\epsilon_{eff} + 2\epsilon_{host}} = f_1\frac{\epsilon_1 - \epsilon_{host}}{\epsilon_1 + 2\epsilon_{host}} + f_2\frac{\epsilon_2 - \epsilon_{host}}{\epsilon_2 + 2\epsilon_{host}} \tag{2.69}$$

In the case of layered media, the continuity of tangential and normal components of the mesoscopic electric field leads to different effective dielectric constants. Tangential fields

Figure 2.8: Material composed of dielectric layers (adapted from Shalaev [43])

lead $\epsilon_{\|}$, and along the symmetry axis normal fields lead to $\epsilon_{\perp}$. If the thickness of the metal is t_m and the dielectric is t_d for a metal-dielectric layer. [35]

$$f_a = \frac{t_m}{t_m + t_d} \tag{2.70}$$

$$f_b = 1 - f_a \tag{2.71}$$

$$\epsilon_{\|} = f_a\epsilon_a + f_b\epsilon_b \tag{2.72}$$

$$\frac{1}{\epsilon_{\perp}} = \frac{f_a}{\epsilon_a} + \frac{f_b}{\epsilon_b} \tag{2.73}$$

The material is isotropic in the mesoscopic level, but behaves anisotropic in the macroscopic level. Due to cylindrical symmetry of metal-dielectric layers, layered Hyperbolic Metamaterials (l-HMM) are uniaxial. These approximations are valid only if *Wiener limits* hold.

$$\sum_i f_i\epsilon_i \geq \epsilon_{eff} \geq \left[\sum_i \frac{f_i}{\epsilon_i}\right]^{-1} \tag{2.74}$$

In a realistic l-HMM configuration [34], the layer thicknesses should be at least smaller than $\lambda/10$ for effective medium approximation to be valid.

2.4.3 Hyperbolic Dispersion Relations in Metal-Dielectric Layers

The dispersion relation for an isotropic dielectric is linear in 1D and comprises an isofrequency contour of a sphere in 3D k-space.

$$k_x^2 + k_y^2 + k_z^2 = (\frac{\omega}{c})^2 \tag{2.75}$$

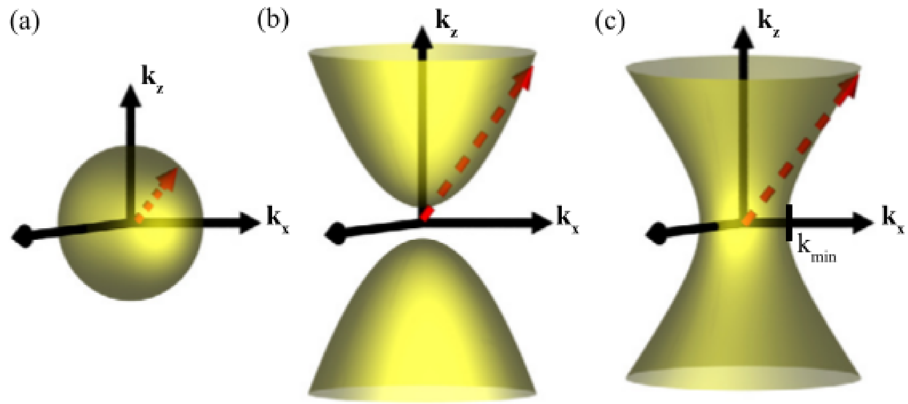

Figure 2.9: k-space isofrequency plots for a) an isotropic dielectric; sphere. b)type-1 l-HMM, $\epsilon_{xx} = \epsilon_{yy} = \epsilon_{\|} > 0$ and $\epsilon_{zz} = \epsilon_{\perp} < 0$; hyperboloid. c)type-2 l-HMM,$\epsilon_{\|} < 0$ and $\epsilon_{\perp} > 0$; hyperboloid. Waves in a) are bounded, but l-HMMs in b) and c) are not. They can support high-k states. (adapted from Zubin Jacob Q.Hyp [35])

Due to surface plasmon resonances induced in respective surfaces of metal-dielectric layers and extreme anisotropy ($\epsilon_{\perp}\epsilon_{\|} < 0$), which is nowhere to be found in nature, l-HMMs have a spectacular dispersion relation. Their uniaxial electromagnetic response is dielectric ($\epsilon > 0$) on one direction, and metalic ($\epsilon < 0$) on the other direction.

$$\hat{\varepsilon} = \begin{bmatrix} \epsilon_{\|} & 0 & 0 \\ 0 & \epsilon_{\|} & 0 \\ 0 & 0 & \epsilon_{\perp} \end{bmatrix} \tag{2.76}$$

$$\frac{k_x^2 + k_y^2}{\epsilon_{\perp}} + \frac{k_z^2}{\epsilon_{\|}} = (\frac{\omega}{c})^2 \tag{2.77}$$

Since isofrequency surfaces of both types of l-HMMs are not bounded in k-space, they can support very high-k states. These high-k states are normally lost due to their evanescent character in usual dielectrical media such that the visual information carried by these states are as well gone, resulting in diffraction limit, $k\ 1/\lambda$. In the l-HMM, on the other hand, they are neither lost, nor partly-evanescent like Pendry's proposal [24]. There are in fact propagating, and many hyperlens proposals [31] [49] are based on this property. Yet, no one ever accomplished outcoupling [50] these high-k modes to vacuum.

2.5 Field Distribution and Purcell Effect inside l-HMMs

The Green's tensor in k-space for an electrical dipole (atom) embedded in layered dielectrical media with hyperbolic dispersion [45] [51] [52] , and uniaxial anisotropy, is as follows. For $k = \omega/c$, $q_{\|} = q_x^2 + q_y^2$ and $q_{\perp}^2 = q_z^2$,

$$\hat{\mathbf{G}}(\mathbf{r}) = \int \frac{d^3q}{(2\pi)^3}\hat{\mathbf{G}}(\mathbf{q}) \tag{2.78}$$

$$\hat{\mathbf{G}}(\mathbf{q}) = 4\pi k^2 \Bigg\{ \left(\epsilon_{\|}\epsilon_{\perp}\hat{\varepsilon} - \frac{\mathbf{q}\otimes\mathbf{q}}{k^2}\right)\frac{1}{q_{\perp}^2\epsilon_{\perp} + q_{\|}^2\epsilon_{\|} - k^2\epsilon_{\|}\epsilon_{\perp}} + \tag{2.79}$$

$$\frac{(\mathbf{q}\times\hat{\mathbf{z}})\otimes(vbq\times\hat{\mathbf{z}})}{q_{\|}^2}\left(\frac{1}{q^2 - k^2\epsilon_{\|}} - \frac{\epsilon_{\perp}}{q_{\perp}^2\epsilon_{\perp} + q_{\|}^2\epsilon_{\|}}\right)\Bigg\} \tag{2.80}$$

Where $\times$ denotes dyadic product, $\otimes$ denotes direct product, $[a\otimes b]\alpha\beta = a_\alpha b_\beta$, and $\hat{\varepsilon}$ denotes dielectric tensor. First pole in this equation corresponds to TM and second pole to TE polarized electrical field. According to [53] [52] [53] , Green's tensor in position space is given as,

$$\begin{aligned}
\hat{\mathbf{G}}(\mathbf{r}) = \hat{\mathbf{G}}_{sing}(\mathbf{r}) + \frac{1}{\sqrt{\varepsilon_{\|}}}\Bigg\{ & k^2\frac{e^{ikr_e}}{r_e}\left(1 - \frac{1}{ikr_e} - \frac{1}{k^2r_e^2}\right)\hat{\epsilon} \\
& -k^2\frac{e^{ikr_e}}{r_e^3}\left(1 - \frac{3}{ikr_e} - \frac{3}{k^2r_e^2}\right)(\hat{\epsilon}\mathbf{r})\otimes(\hat{\epsilon}\mathbf{r}) \\
& +k^2\left(\varepsilon_{\|}\frac{e^{ikr_o}}{r_o} - \varepsilon_{\perp}\frac{e^{ikr_e}}{r_e}\right)\frac{(\mathbf{r}\times\hat{\mathbf{z}})\otimes(\mathbf{r}\times\hat{\mathbf{z}})}{(\mathbf{r}\times\hat{\mathbf{z}})^2} \\
& -ik\frac{e^{ikr_o} - e^{ikr_e}}{(\mathbf{r}\times\hat{\mathbf{z}})^2}\left(\hat{\mathbf{I}} - \hat{\mathbf{z}}\otimes\hat{\mathbf{z}} - 2\frac{(\mathbf{r}\times\hat{\mathbf{z}})\otimes(\mathbf{r}\times\hat{\mathbf{z}})}{(\mathbf{r}\times\hat{\mathbf{z}})^2}\right)\Bigg\}
\end{aligned} \tag{2.81}$$

$$\begin{aligned}
\hat{\mathbf{G}}_{sing}(\mathbf{r}) &= \left[(\boldsymbol{\nabla}\otimes\boldsymbol{\nabla})\frac{1}{\sqrt{\varepsilon_{\|}r_e}}\right]_{sing} \\
&= \left[\int\frac{d^3q}{(2\pi)^2}e^{i\mathbf{q}\cdot\mathbf{r}}\frac{\mathbf{q}\otimes\mathbf{q}}{q_{\perp}^2\varepsilon_{\perp} + q_{\|}^2\varepsilon_{\|}}\right]_{sing}
\end{aligned} \tag{2.82}$$

Where, $\hat{\epsilon} = \varepsilon_{\|}\varepsilon_{\perp}(\hat{\varepsilon})^{-1}$, $r_e = \sqrt{\mathbf{r}\hat{\epsilon}\mathbf{r}}$, and, $r_o = \sqrt{\varepsilon_{\|}}$. As we will see in later sections, Purcell factor [44], the term determines enhancement of spontaneous emission rate in l-HMM with respect to vacuum, $\Gamma = f\Gamma_0$, can be calculated using Green's tensor. Once the singularities are smeared out [45] by using test function of a Gaussian of width a, Purcell factor for dipole oriented in $\hat{n}$ direction is given as,

$$f = \frac{3}{2k^3} Im\left[Tr[\mathbf{G}(\mathbf{r}_0, \mathbf{r}_0)]_{\hat{n}}\right] = \frac{3}{2k^3} Im[\hat{\mathbf{n}} \cdot G(0) \cdot \hat{\mathbf{n}}]$$
$$= \sqrt{\varepsilon_\parallel} - \frac{3\sqrt{\pi\varepsilon_\parallel}(2\varepsilon_\parallel + |\varepsilon_\perp|)}{8ka(\varepsilon_\parallel + |\varepsilon_\perp|)^{3/2}} + \frac{3\sqrt{\pi\varepsilon_\parallel}}{8(ka)^3(\varepsilon_\parallel + |\varepsilon_\perp|)^{3/2}} \tag{2.83}$$

As Newman [34] and Liu [32] demonstrated not by using Green's tensor formalism, but FDTD simulations and Wigner-Weisskopf approximation, there is significant increase of spontaneous emission rate inside l-HMM, both for Type 1 and Type 2 with respect to both wavelength and spatial parameter,α,

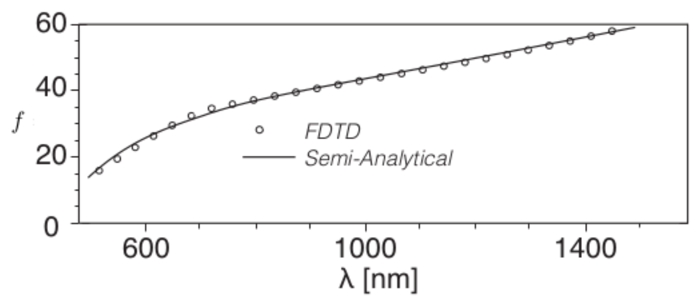

Figure 2.10: Single

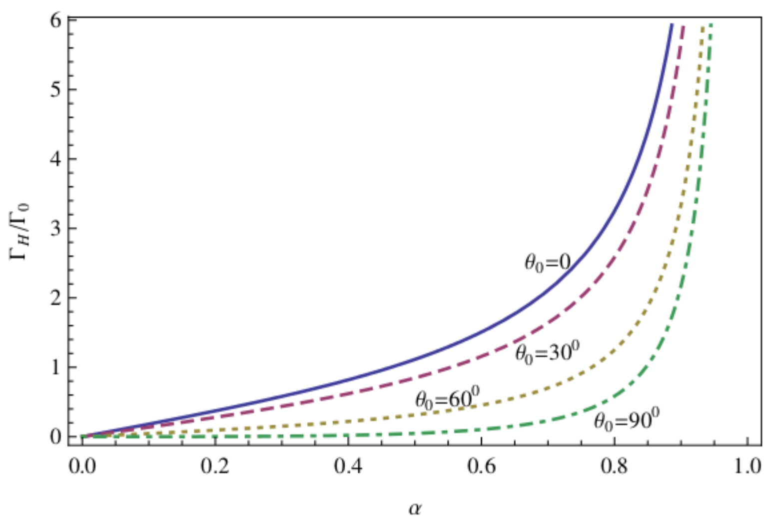

Figure 2.11: Single

By integrating Green's tensor [45] [29] with a point dipole as source current density,

$\mathbf{j}(\mathbf{r}) = \delta(\mathbf{r})\mathbf{p}$, we get the the spatial electric field distributions, $\mathbf{E}(\mathbf{r}) = \int d^3r\mathbf{G}(\mathbf{r}-\mathbf{r}')\delta(\mathbf{r})\mathbf{p}$, for respective polarizations, HMM types and dipole orientations as demonstrated in figures 2.12 2.14 2.13 2.15.

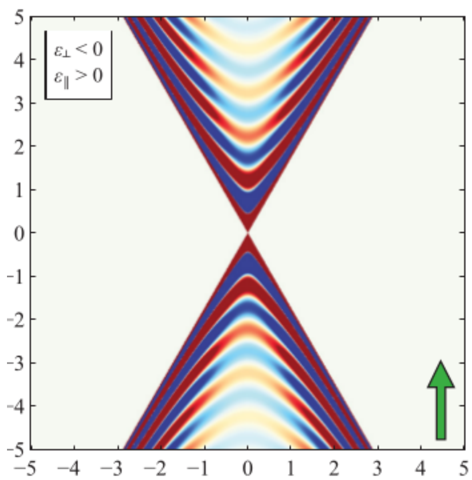

Figure 2.12: Electric field distribution of a dipole embedded in Type 1 l-HMM medium and oriented in $\hat{\mathbf{e}} = \hat{z}$ direction. Adapted from [45]

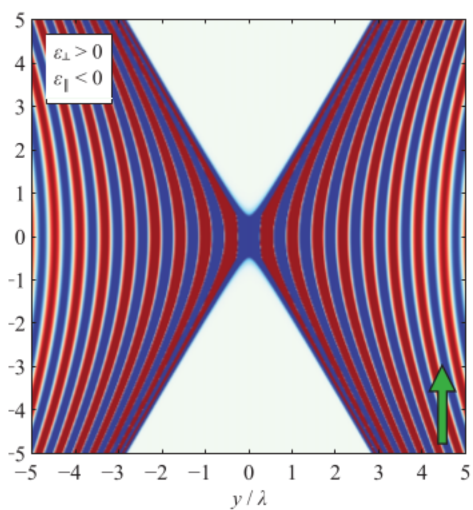

Figure 2.13: Electric field distribution of a dipole embedded in Type 2 l-HMM medium and oriented in $\hat{\mathbf{e}} = \hat{z}$ direction. Adapted from [45])

In figures 2.12 2.14 2.13 2.15, field is either distributed conically, or with a "butterfly" shaped profile where field is emitted to every direction by the dipole, except a conical

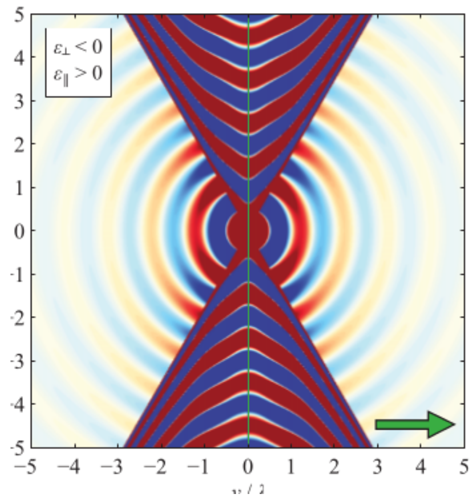

Figure 2.14: Electric field distribution of a dipole embedded in Type 1 l-HMM medium and oriented in $\hat{\mathbf{e}} = \hat{y}$ direction. Adapted from [45])

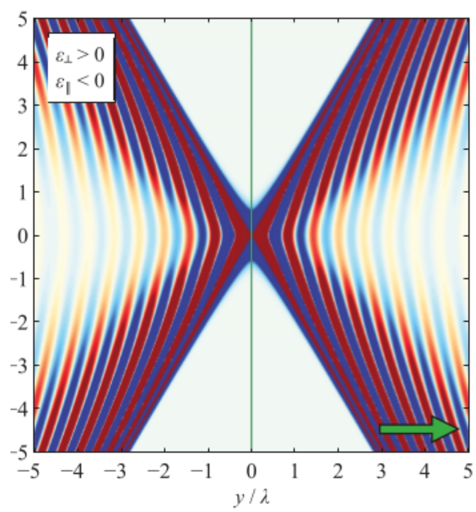

Figure 2.15: Electric field distribution of a dipole embedded in Type 2 l-HMM medium and oriented in $\hat{\mathbf{e}} = \hat{y}$ direction. Adapted from [45])

region, depending on HMM type. This behaviour is known as *Resonance cone* [34] [54] [55] [56] [27] [29] , and field is (not) emitted to a cone of half-angle, $\theta_{RC} = \arctan\left(\left|(\epsilon_\parallel/\epsilon_\perp)\right|\right)$.

Chapter 3

GREEN'S FORMALISM

3.1 The Hopfield Model of Bulk Dielectric

The Hopfield model [37] [14] [57] [58] [59] [60] [61] [62] [63] interprets the bulk dielectric medium as a collection of N harmonic oscillators that correspond to polarization of the medium and a continuum of harmonic oscillator field describing the reservoir. These discrete and continuum fields are linearly coupled to each other by nonsingular, square-integrable coupling constants, and, leading the energy flow to the reservoir, where it is absorbed. The Lagrangian of the total system when radiation is included

$$L = \int d^3\mathbf{r}\mathcal{L} = \int d^3\mathbf{r}(\mathcal{L}_{rad} + \mathcal{L}_{mat} + \mathcal{L}_{int}) \tag{3.1}$$

$$\mathcal{L}_{rad} = \frac{\varepsilon_0}{2}(\mathbf{E}^2 - c^2\mathbf{B}^2) = \frac{\varepsilon_0}{2}[(\dot{\mathbf{A}} + \boldsymbol{\nabla}\phi)^2 - c^2(\boldsymbol{\nabla}\times\mathbf{A})^2] \tag{3.2}$$

$$\mathcal{L}_{mat} = \frac{\mu}{2}[\sum_{i=1}^{N}(\dot{\mathbf{X}}_i^2 - \omega_i^2\mathbf{X}_i^2) + \int\limits_0^\infty d\omega(\dot{\mathbf{X}}(\omega)^2 - \omega^2\mathbf{X}(\omega)^2] \tag{3.3}$$

$$\mathcal{L}_{int} = -\sum_{i=1}^{N}\alpha_i(\mathbf{A}\dot{\mathbf{X}}_i + \phi\boldsymbol{\nabla}\cdot\mathbf{X}_i) - \int\limits_0^\infty d\omega\dot{\mathbf{X}}(\omega)\sum_{i=1}^{N}\upsilon_i(\omega)\mathbf{X}_i \tag{3.4}$$

Where $\mathbf{X}_i$ is medium oscillator field for polarization, $\mathbf{X}(\omega)$ is continuous reservoir oscillator field, α is medium polarizability and $\upsilon(\omega$ is medium-reservoir coupling term. Since $\frac{\partial\mathcal{L}}{\partial\dot{\phi}} = 0$, ϕ, the scalar potential is a redundant variable, which can be eliminated within Coulomb Gauge ($\boldsymbol{\nabla}\cdot\mathbf{A} = 0$) using Euler-Lagrange equations of motion (correspond to Maxwell equations in this case). If we go to reciprocal space by using 3D Fourier transformations,using the fact that for real fields $\mathbf{E}(\mathbf{r})$, $\underline{\mathbf{E}}^*(\mathbf{k}) = \underline{\mathbf{E}}(-\mathbf{k})$,

$$\mathbf{E}(\mathbf{r},t) = \int \frac{d^3k}{(2\pi)^{\frac{3}{2}}} \underline{\mathbf{E}}(\mathbf{k},t) e^{i\mathbf{k}\cdot\mathbf{r}} \tag{3.5}$$

$$\underline{\mathcal{L}}_{int} = -\sum_{i=0}^{N} \left\{ \alpha \left[\underline{\mathbf{A}}^* \cdot \dot{\underline{\mathbf{X}}}_i + \underline{\mathbf{A}} \cdot \dot{\underline{\mathbf{X}}}_i^* + i\mathbf{k} \cdot \left(\underline{\phi}^* \cdot \underline{\mathbf{X}}_i - \underline{\phi} \cdot \underline{\mathbf{X}}_i^* \right) \right] \right. \tag{3.6}$$

$$\left. - \int_0^\infty d\omega v(\omega) \left(\underline{\mathbf{X}}_i^* \cdot \dot{\underline{\mathbf{X}}}(\omega) + \underline{\mathbf{X}}_i \cdot \dot{\underline{\mathbf{X}}}(\omega)^* \right) \right\} \tag{3.7}$$

Equation of motion for the variable $\dot{\underline{\phi}}^*(\mathbf{k})$ can then be used to eliminate $\underline{\phi}$

$$\underline{\phi} = i\frac{\alpha}{\varepsilon_0} \left(\frac{\kappa \cdot \underline{\mathbf{X}}_i(\mathbf{k},t)}{\mathbf{k}} \right) \tag{3.8}$$

Coulomb gauge condition in reciprocal space, $\mathbf{k} \cdot \underline{\mathbf{A}}(\mathbf{k},t) = 0$, makes $\mathbf{A}$ a purely transverse field so that we can separate transverse and longitudinal parts of the fields. Using $\kappa = \frac{\mathbf{k}}{|\mathbf{k}|}$, $\mathbf{e}_\lambda(\mathbf{k}) \perp \mathbf{k}$,

$$\mathbf{A}(\mathbf{r}) \to \tilde{\mathbf{A}}(\mathbf{k}) = \sum_{\lambda=1}^{2} A_\lambda(\mathbf{k}) \mathbf{e}_\lambda(\mathbf{k}) \tag{3.9}$$

$$\mathbf{X}_i(\mathbf{r}) \to X_{i\|}(\mathbf{k})\kappa + \sum_{\lambda=1}^{2} X_{i\lambda}(\mathbf{k}) \mathbf{e}_\lambda(\mathbf{k}) \tag{3.10}$$

$$L = \int d^3k \mathcal{L}^\perp + \mathcal{L}^\| \tag{3.11}$$

$$\mathcal{L}_{rad}^\perp = \varepsilon_0 \left(|\dot{\mathbf{A}}|^2 - c^2k^2|\mathbf{A}|^2 \right) \tag{3.12}$$

$$\mathcal{L}_{mat}^\perp = \sum_{i=0}^{N} \mu \left[|\dot{\mathbf{X}}_i^\perp|^2 - \omega_i \mathbf{X}_i^\perp|^2 + \int_0^\infty d\omega \left(|\dot{\mathbf{X}}^\perp(\omega)|^2 - \omega \mathbf{X}^\perp(\omega)|^2 \right) \right] \tag{3.13}$$

$$\mathcal{L}_{int}^\perp = -\sum_{i=0}^{N} \left[\alpha \mathbf{A} \cdot \dot{\mathbf{X}}_i^{\perp *} + \int_0^\infty d\omega v(\omega) \mathbf{X}_i^{\perp *} \cdot \dot{\mathbf{X}}^{\perp *}(\omega) + c.c. \right] \tag{3.14}$$

$$\mathcal{L}^\| = \sum_{i=0}^{N} \mu \left\{ |\dot{\mathbf{X}}_i^\||^2 - \tilde{\omega}_{i\|}^2 |\mathbf{X}_i|^2 + \int_0^\infty d\omega \left(|\dot{\mathbf{X}}^\|(\omega)|^2 - \omega \mathbf{X}^\|(\omega)|^2 \right) \right. \tag{3.15}$$

$$\left. + \int_0^\infty d\omega v(\omega) \left(\mathbf{X}_i^{\|*} \cdot \dot{\mathbf{X}}^{\|*}(\omega) + c.c. \right) \right\} \tag{3.16}$$

Where $\tilde{\omega}_{i\|}^2 = \tilde{\omega}_i^2 + \frac{\alpha_i^2}{\mu\varepsilon_0}$. To obtain the Hamiltonian, we make a Legendre transformation by obtaining canonical coordinates and momenta,

$$\mathbf{\Pi} = \frac{\partial \mathcal{L}}{\partial \dot{\mathbf{A}}} = \varepsilon_0 \dot{\mathbf{A}} \tag{3.17}$$

$$\mathbf{Q}_i = \frac{\partial \mathcal{L}}{\partial \dot{\mathbf{X}}_i} = \mu \dot{\mathbf{X}}_i - \alpha_i \mathbf{A} \tag{3.18}$$

$$\mathbf{Q}(\omega) = \frac{\partial \mathcal{L}}{\partial \dot{\mathbf{X}}(\omega)} = \mu \dot{\mathbf{X}}(\omega) - \sum_{i=1}^{N} \upsilon_i(\omega) \mathbf{X}_i \tag{3.19}$$

Having obtained the canonical variables, a canonical transformation to obtain complex field amplitudes for transverse and longitudinal can be made by defining $\tilde{k}^2 = k^2 + \sum_{i=1}^{N} \frac{\alpha_i^2}{\mu\varepsilon_0 c^2}$ and $\tilde{\omega}^2 = \omega_i^2 + \int_0^\infty d\omega \frac{\upsilon_i^2(\omega)}{\mu^2}$,

$$a_\lambda(\mathbf{k}) = \sqrt{\frac{\varepsilon_0}{2\hbar\tilde{k}c}} \left[\tilde{k}cA_\lambda(\mathbf{k}) + \frac{i}{\varepsilon_0} \Pi_\lambda(\mathbf{k}) \right] \tag{3.20}$$

$$b_{i\lambda}(\mathbf{k}) = \sqrt{\frac{\mu}{2\hbar\tilde{\omega}_i}} \left[\tilde{\omega}_i X_{i\lambda}(\mathbf{k}) + \frac{i}{\mu} Q_{i\lambda}(\mathbf{k}) \right] \tag{3.21}$$

$$b_\lambda(\mathbf{k},\omega) = \sqrt{\frac{\mu}{2\hbar\omega}} \left[-i\omega X_\lambda(\mathbf{k},\omega) + \frac{1}{\mu} Q_\lambda(\mathbf{k},\omega) \right] \tag{3.22}$$

$$b_{i\|}(\mathbf{k}) = \sqrt{\frac{\mu}{2\hbar\tilde{\omega}_{i\|}}} \left[\tilde{\omega}_i X_{i\|}(\mathbf{k}) + \frac{i}{\mu} Q_{i\|}(\mathbf{k}) \right] \tag{3.23}$$

$$b_\|(\mathbf{k},\omega) = \sqrt{\frac{\mu}{2\hbar\omega}} \left[-i\omega X_\|(\mathbf{k},\omega) + \frac{1}{\mu} Q_\|(\mathbf{k},\omega) \right] \tag{3.24}$$

If we change these complex amplitudes with bosonic creation(annihilation) operators, quantization scheme is complete to gather Hamiltonian operator,

$$\hat{H} = \hat{H}^\perp + \hat{H}_{mat}^\| \qquad \hat{H}^\perp = \hat{H}_{rad} + \hat{H}_{mat}^\perp + \hat{H}_{int}^\perp \tag{3.25}$$

For $V_i(\omega) = (\upsilon_i(\omega)/\mu)(\omega/\tilde{\omega}_i)^{1/2}$ and $\Lambda_i(k) = [(\tilde{\omega}_i \alpha_i^2)/(\mu c \varepsilon_0 \tilde{k})]^{1/2}$,

$$\hat{H}_{mat}^{\parallel} = \int d^3\mathbf{k} \Bigg\{ \int_0^\infty d\omega \hbar\omega \hat{b}_{\parallel}^{\dagger}(\mathbf{k},\omega)\hat{b}_{\parallel}(\mathbf{k},\omega) + \sum_{i=1}^{N} \hbar\tilde{\omega}_{i\parallel}\hat{b}_{i\parallel}^{\dagger}(\mathbf{k})\hat{b}_{i\parallel}(\mathbf{k}) + \int_0^\infty d\omega \sum_{i=1}^{n} \left[\frac{1}{2}\hbar V_i(\omega)\left(\hat{b}_{i\parallel}^{\dagger}(\mathbf{k}) + \hat{b}_{i\parallel}(-\mathbf{k})\right)\left(\hat{b}_{\parallel}^{\dagger}(-\mathbf{k},\omega) + \hat{b}_{\parallel}(\mathbf{k},\omega)\right)\right]\Bigg\} \tag{3.26}$$

$$\hat{H}_{rad}^{\perp} = \sum_{\lambda=1}^{2} \int d^3\mathbf{k} \hbar\tilde{k}c\hat{a}_{\lambda}^{\dagger}(\mathbf{k})\hat{a}_{\lambda}(\mathbf{k}) \tag{3.27}$$

$$\hat{H}_{mat}^{\perp} = \sum_{\lambda=1}^{2} \int d^3\mathbf{k} \Bigg\{ \int_0^\infty d\omega \hbar\omega \hat{b}_{\lambda}^{\dagger}(\mathbf{k},\omega)\hat{b}_{\lambda}(\mathbf{k},\omega) + \sum_{i=1}^{N} \hbar\tilde{\omega}_{i}\hat{b}_{i\lambda}^{\dagger}(\mathbf{k})\hat{b}_{i\lambda}(\mathbf{k}) + \int_0^\infty d\omega \sum_{i=1}^{n} \Bigg[\tfrac{1}{2}\hbar V_i(\omega)\left(\hat{b}_{i\lambda}^{\dagger}(\mathbf{k}) + \hat{b}_{i\lambda}(-\mathbf{k})\right)\left(\hat{b}_{\lambda}^{\dagger}(-\mathbf{k},\omega) + \hat{b}_{\lambda}(\mathbf{k},\omega)\right) + \sum_{j\neq i} \tfrac{1}{2}\hbar V_i(\omega)V_j(\omega)\left(\hat{b}_{i\lambda}^{\dagger}(\mathbf{k}) + \hat{b}_{i\lambda}(-\mathbf{k})\right)\left(\hat{b}_{j\lambda}^{\dagger}(-\mathbf{k},\omega) + \hat{b}_{j\lambda}(\mathbf{k},\omega)\right)\Bigg]\Bigg\} \tag{3.28}$$

$$\hat{H}_{int}^{\perp} = \sum_{\lambda=1}^{2}\sum_{i=1}^{N} \int d^3\mathbf{k} \tfrac{1}{2} i\hbar\Lambda_i(k)\left[\hat{a}_{\lambda}^{\dagger}(-\mathbf{k}) + \hat{a}_{\lambda}(\mathbf{k})\right]\left[\hat{b}_{i\lambda}^{\dagger}(\mathbf{k}) + \hat{b}_{i\lambda}(-\mathbf{k})\right] \tag{3.29}$$

3.1.1 Fano Diagonalization

The diagonalization procedure of the Hamiltonian starts, first, by a Fano [13] type diagonalization [64] of the longitudinal matter part. The derivation of all the parameters is rather lengthy for the scope of this thesis, but the essence is as follows. The procedure begins by defining dressed matter field, $\hat{B}(\mathbf{k},\omega)$,

$$\hat{H}^{\|}_{mat} = \int d^3\mathbf{k} \int_0^\infty d\omega \hbar\omega \hat{B}^\dagger(\mathbf{k},\omega)\hat{B}(\mathbf{k},\omega) \tag{3.30}$$

$$\left[\hat{B}(\mathbf{k},\omega), \hat{B}^\dagger(\mathbf{k}',\omega')\right] = \delta(\mathbf{k}-\mathbf{k}')\delta(\omega-\omega') \tag{3.31}$$

$$\begin{aligned}\hat{B}(\mathbf{k},\omega) &= \alpha_0(\omega)\hat{b}_{i\|}(\mathbf{k}) + \beta_0(\omega)\hat{b}^\dagger_{i\|}(-\mathbf{k}) \\ +\int_0^\infty d\omega' &\left[\alpha_1(\omega,\omega')\hat{b}_\|(\mathbf{k},\omega') + \beta_1\omega,\omega')\hat{b}^\dagger_\|(-\mathbf{k},\omega')\right]\hat{b}_{i\|}(\mathbf{k}) \\ &= \int_0^\infty d\omega \left[\alpha_0^*\hat{B}(\mathbf{k},\omega) - \beta_0\hat{B}^\dagger(-\mathbf{k},\omega)\right]\end{aligned} \tag{3.32}$$

$$\hat{b}_\|(\mathbf{k},\omega) = \int_0^\infty d\omega' \left[\alpha_1^*(\omega',\omega)\hat{B}(\mathbf{k},\omega') - \beta_1(\omega',\omega)\hat{B}^\dagger(-\mathbf{k},\omega')\right] \tag{3.33}$$

$$\begin{aligned}\left[\hat{b}_{i\|}(\mathbf{k}), \hat{b}^\dagger_{i\|}(\mathbf{k}')\right] &= \delta(\mathbf{k}-\mathbf{k}')I_1 \\ &= \delta(\mathbf{k}-\mathbf{k}')\int_0^\infty d\omega[|\alpha_0|^2 - |\beta_0|^2]\end{aligned} \tag{3.34}$$

$$\begin{aligned}\left[\hat{b}_\|(\mathbf{k},\omega), \hat{b}^\dagger_\|(\mathbf{k}',\omega')\right] &= \delta(\mathbf{k}-\mathbf{k}')I(\omega,\omega') \\ = \delta(\mathbf{k}-\mathbf{k}')\int_0^\infty d\nu[\alpha_1^*(\nu,\omega)&\alpha_1(\nu,\omega') - \beta_1(\nu,\omega)\beta_1^*(\nu,\omega')]\end{aligned} \tag{3.35}$$

Commutation relations [63] are satisfied if and only if $I_1 = 1$ and $I(\omega,\omega') = \delta(\omega-\omega')$. Similarly, the transverse part of the Hamiltonian, which includes transverse matter modes and radiation field, can be diagonalized by Fano method, this time defining $g(\omega) = i(\alpha_0(\omega) + \beta_0(\omega))$ and polaritonic operators $\hat{C}(\mathbf{k},\omega)$,

$$H^\perp_{int} = \frac{\hbar}{2}\Lambda_i(\omega)\int_0^\infty d\omega \left\{g(\omega)\hat{B}^\dagger(\mathbf{k},\omega)\left[\hat{a}(\mathbf{k}) + \hat{a}^\dagger(-\mathbf{k})\right]\right\} \tag{3.36}$$

Diagonalized $H^{\parallel}_{mat}$ results are used to diagonalize the rest,

$$\hat{H}^{\perp} = \sum_{\lambda=1}^{2} \int d^3\mathbf{k} \int_0^{\infty} d\omega \hbar\omega \hat{C}^{\dagger}_{\lambda}(\mathbf{k},\omega)\hat{C}_{\lambda}(\mathbf{k},\omega) \tag{3.37}$$

$$\hat{C}_{\lambda}(\mathbf{k},\omega) = \tilde{\alpha}_0(k,\omega)\hat{a}(\mathbf{k}) + \tilde{\beta}_0(k,\omega)\hat{a}^{\dagger}(-\mathbf{k})$$
$$+ \int_0^{\infty} d\omega' \left[\tilde{\alpha}_1(k,\omega,\omega')\hat{B}(\mathbf{k},\omega') + \tilde{\beta}_1(k,\omega,\omega')\hat{B}^{\dagger}(-\mathbf{k},\omega')\right] \tag{3.38}$$

$$\left[\hat{C}_{\lambda}(\mathbf{k},\omega), \hat{C}^{\dagger}_{\lambda}(\mathbf{k}',\omega')\right] = \delta(\mathbf{k}-\mathbf{k}')\delta(\omega-\omega') \tag{3.39}$$

By imposing the commutation relations, α_0, $\alpha_1(\omega,\omega')$, β_0, $\beta_1(\omega,\omega')$, $\tilde{\alpha_0}$, $\alpha_1(\tilde{\omega,\omega'})$, $\tilde{\beta_0}$, $\beta_1(\tilde{\omega,\omega'})$ parameters are found so that the quantum mechanical vector potential of the overall system is,

$$\hat{\hat{\mathbf{A}}}(\mathbf{k}) = -\sum_{\lambda=1}^{2} \hat{\mathbf{e}}_{\lambda}(\mathbf{k}) \sqrt{\frac{\hbar}{\pi\varepsilon_0}} \int_0^{\infty} d\omega\omega\sqrt{\varepsilon_I(\omega)}\tilde{G}(\mathbf{k},\omega)\hat{C}_{\lambda}(\mathbf{k},\omega) + H.C \tag{3.40}$$

Where $\tilde{G}(\mathbf{k},\omega)$ is the reciprocal space Green's tensor of macroscopical electric field in bulk dielectric,

$$\tilde{G}(\mathbf{k},\omega) = -\frac{c^2}{\omega^2\varepsilon(\omega) - k^2c^2} \tag{3.41}$$

The overall polarization in the bulk dielectric medium is,

$$\hat{\hat{P}}(\mathbf{k}) = \sum_{\lambda=1}^{2}\sum_{i=1}^{N} \alpha_i \hat{\mathbf{X}}_{i\lambda}(\mathbf{k})$$
$$= -i\sum_{\lambda=1}^{2}\sqrt{\frac{\hbar\varepsilon_0}{\pi}} \left[\int_0^{\infty} d\omega\omega^2[\varepsilon(\omega)-1]\sqrt{\varepsilon_I(\omega)}\tilde{G}(\mathbf{k},\omega)\hat{C}_{\lambda}(\mathbf{k},\omega) + H.C\right]$$
$$+\hat{\hat{P}}_N(\mathbf{k}) \tag{3.42}$$

First part of the polarization corresponds to induced polarization. Though, the second part is *noise* polarization, which is the fluctuating part related to absorption in the media,

$$\hat{\hat{P}}_N(\mathbf{k}) = \sum_{\lambda=1}^{2}\sqrt{\frac{\hbar\varepsilon_0}{\pi}} \int_0^{\infty} d\omega i\sqrt{\varepsilon_I}\hat{C}_{\lambda}(\mathbf{k},\omega) + H.C \tag{3.43}$$

To sum up, electromagnetic fields can be quantized without referencing any microscopical model. A source quantity representation of macroscopical electric field with classical Green's function and permittivities and a continuum of harmonic oscillators standing as a reservoir are enough to give a picture of quantum electrodynamics inside bulk dielectrics, which can be generalized to any dielectric media.

3.2 The Medium Assisted Maxwell Field

We start by macroscopical Maxwell equations stated in chapter 2, and phenomenological dielectric functions obtained from measurements, which contains most of the knowledge regarding media, including reservoir. By adding noise polarization terms obtained in section 1 to overall polarization we have,

$$\mathbf{P}(\mathbf{r},t) = \int_t^\infty dt' \chi(\mathbf{r}, t-t')\mathbf{E}(\mathbf{r},t') + \hat{\hat{P}}_N(\mathbf{k}) \tag{3.44}$$

$$\mathbf{D}(\mathbf{r},t) = \varepsilon_0 \mathbf{E}(\mathbf{r},t) + \mathbf{P}_N(\mathbf{r},t) \tag{3.45}$$

Noise charge and current densities are obtained,

$$\varepsilon_0 \boldsymbol{\nabla} \cdot (\varepsilon(\mathbf{r},\omega)\mathbf{E}(\mathbf{r},\omega)) = \rho_N(\mathbf{r},\omega) \tag{3.46}$$

$$\boldsymbol{\nabla} \times \mathbf{B}(\mathbf{r},\omega) + i\tfrac{\omega}{c^2}\varepsilon(\mathbf{r},\omega)\mathbf{E}(\mathbf{r},\omega) = \mu_0 j_N(\mathbf{r},\omega) \tag{3.47}$$

Continuity condition must be satisfied,

$$\rho_N(\mathbf{r},\omega) = -\boldsymbol{\nabla} \cdot \mathbf{P}_N(\mathbf{r},\omega); \mathbf{j}_N(\mathbf{r},\omega) = -i\omega \mathbf{P}_N(\mathbf{r},\omega) \tag{3.48}$$

$$\boldsymbol{\nabla} \cdot \mathbf{j}_N(\mathbf{r},\omega) - i\omega\rho_N(\mathbf{r},\omega) = 0 \tag{3.49}$$

Adding noise polarization,

$$\mathbf{E}(\mathbf{r},\omega) = i\omega\mu_0 \int d^3\mathbf{r}' \mathbf{G}(\mathbf{r},\mathbf{r}',\omega)\mathbf{j}_N(\mathbf{r}',\omega) \tag{3.50}$$

Fourier components of magnetic induction and electric displacement are directly related to Fourier component of electric field,

$$\mathbf{B}(\mathbf{r},\omega) = (i\omega)^{-1}\boldsymbol{\nabla} \times \mathbf{E}(\mathbf{r},\omega) \tag{3.51}$$

$$\mathbf{D}(\mathbf{r},\omega) = (\mu_0\omega^2)^{-1}\boldsymbol{\nabla} \times \boldsymbol{\nabla} \times \mathbf{E}(\mathbf{r},\omega) \tag{3.52}$$

Continuous, complex field amplitudes $f(\mathbf{r},\omega)$ can be associated with Fourier components of noise polarization and current terms.They provide a dynamical picture of the radiation field, the medium it linearly interacts and the dissipation process inside this medium.

$$\mathbf{P}_N(\mathbf{r},\omega) = i\sqrt{\frac{\hbar\varepsilon_0}{\pi}\varepsilon_I(\mathbf{r},\omega)}\mathbf{f}(\mathbf{r},\omega) \tag{3.53}$$

3.2.1 Quantization of Medium Assisted Field

If we are to change complex field amplitudes in Fourier components of noise polarization with Bosonic creation(annihilation) operators and impose usual commutation relation condition,

$$\left[\hat{f}_k(\mathbf{r},\omega), \hat{f}^{\dagger}_{k'}(\mathbf{r}',\omega')\right] = \delta_{kk'}\delta(\mathbf{r}-\mathbf{r}')\delta(\omega-\omega') \tag{3.54}$$

$$\left[\hat{f}_k(\mathbf{r},\omega), \hat{f}_{k'}(\mathbf{r}',\omega')\right] = \left[\hat{f}^{\dagger}_k(\mathbf{r},\omega), \hat{f}^{\dagger}_{k'}(\mathbf{r}',\omega')\right] = 0 \tag{3.55}$$

The total energy of medium assisted Maxwelll field can be expressed by means of these Bosonic operators,

$$\hat{H} = \int d^3\mathbf{r} \int_0^{\infty} d\omega\hbar\omega\hat{\mathbf{f}}^{\dagger}(\mathbf{r},\omega)\hat{\mathbf{f}}(\mathbf{r},\omega) \tag{3.56}$$

Fourier component of electric field operator can be obtained by plugging medium-assisted field operator, classical Green's dyad and imaginary part of dielectric function into above equations, and magnetic field component is easily obtained,

$$\hat{\mathbf{E}}(\mathbf{r},\omega) = i\frac{\hbar\varepsilon}{\pi}\left(\frac{\omega}{c}\right)^2 \int d^3\mathbf{r}'\sqrt{\varepsilon_I(\mathbf{r}',\omega)}\mathbf{G}(\mathbf{r},\mathbf{r}',\omega)\hat{\mathbf{f}}(\mathbf{r},\omega) \tag{3.57}$$

$$\hat{\mathbf{B}}(\mathbf{r},\omega) = (i\omega)^{-1}\nabla\times\hat{\mathbf{E}}(\mathbf{r},\omega) \tag{3.58}$$

Negative frequency(counter-rotating) parts of electric field operator must also be added,

$$\hat{\mathbf{E}}(\mathbf{r}) = \int_0^{\infty} d\omega\hat{\mathbf{E}}(\mathbf{r},\omega) + H.c \tag{3.59}$$

$$\hat{\mathbf{B}}(\mathbf{r}) = \int_0^{\infty} d\omega\hat{\mathbf{B}}(\mathbf{r},\omega) + H.c \tag{3.60}$$

Well-known commutation relations between electric and magnetic field operators also hold because of the properties of Green's tensor and permittivity,

$$\left[\varepsilon_0 \hat{E}_k(\mathbf{r}), \hat{B}_l(\mathbf{r}')\right] = -i\hbar\epsilon_{klm}\partial^r_m \delta(\mathbf{r}-\mathbf{r}') \tag{3.61}$$

$$\left[\hat{E}_k(\mathbf{r}), \hat{E}_l(\mathbf{r}')\right] = \left[\hat{B}_k(\mathbf{r}), \hat{B}_l(\mathbf{r}')\right] = 0 \tag{3.62}$$

3.2.2 Heisenberg Dynamics of Atom-Field Interaction

Bringing the Hamiltonian for interaction between medium-assisted field and an atom is a rather lengthy discussion beyond the scope of this thesis, so we omit the most part. However, after a series of gauge transformations and basis changes we have the usual form,

$$\hat{H} = \hat{H}_A + \hat{H}_M + \hat{H}_{int} \tag{3.63}$$

$$\hat{H}_M = \int d^3\mathbf{r} \int_0^\infty d\omega \hbar\omega \hat{\mathbf{f}}^\dagger(\mathbf{r},\omega)\hat{\mathbf{f}}(\mathbf{r},\omega) \tag{3.64}$$

$$\hat{H}_A = \sum_\alpha \frac{\hat{\mathbf{p}}_\alpha^2}{2m_\alpha} + \tfrac{1}{2}\int d^3\mathbf{r}\hat{\rho}_A(\mathbf{r})\hat{\varphi}_A(\mathbf{r}) \tag{3.65}$$

Where $p_\alpha^2/2m_\alpha$ is kinetic energy of individual atoms and, φ, term is related to Coulomb energy,

$$\hat{\varphi}_A(\mathbf{r}) = \int d^3\mathbf{r}' \frac{\hat{\rho}_A(\mathbf{r}')}{4\pi\varepsilon_0|\mathbf{r}-\mathbf{r}'|} \tag{3.66}$$

$$\hat{\rho}_A(\mathbf{r}) = \sum_\alpha q_\alpha \delta(\mathbf{r}-\hat{\mathbf{r}}_\alpha) \tag{3.67}$$

Interaction Hamiltonian now has the form $\mathbf{p}\cdot\mathbf{A}$,

$$\hat{H}_{int} = -\sum \alpha \frac{q_\alpha}{m_\alpha}\hat{\mathbf{p}}_\alpha \hat{\mathbf{A}}_\alpha(\mathbf{r}_\alpha) + \int d^3\mathbf{r}\hat{\rho}_A(\mathbf{r})\hat{\varphi}_M(\mathbf{r}) \tag{3.68}$$

When dipole-approximation is made, it becomes,

$$-\sum \alpha \frac{q_\alpha}{m_\alpha}\hat{\mathbf{p}}_\alpha \hat{\mathbf{A}}_\alpha(\mathbf{r}_\alpha) = -\frac{1}{i\hbar}\left[\hat{\mathbf{d}}_A, \hat{H}_A\right]\hat{\mathbf{A}}_\alpha(\mathbf{r}_A) \tag{3.69}$$

For a two level system under rotating-wave approximation, we have interaction Hamiltonian of the form $\hat{H}_{int} = \mathbf{d}\cdot\mathbf{E}$,

$$\hat{H}_A = \hbar\omega_u |u\rangle\langle u| + \hbar\omega_l |l\rangle\langle l| = \tfrac{1}{2}\hbar\omega_A\hat{\sigma}_z + const. \tag{3.70}$$

$$\hat{H}_{int} = -\hat{\sigma}^\dagger \hat{\mathbf{E}}_M^{(+)}(\mathbf{r}_A)d + H.c \tag{3.71}$$

Heisenberg equations of motion can be obtained by using commutation relations,

$$\dot{\hat{\mathbf{A}}}(t) = \frac{i}{\hbar}\left[\hat{H}, \hat{\mathbf{A}}(t)\right] \tag{3.72}$$

Coupled differential equations for atomic and field operators are following,

$$\dot{\hat{\sigma}}_z = \frac{2i}{\hbar}\hat{\sigma}^\dagger \hat{\mathbf{E}}_M^{(+)}(\mathbf{r}_A)\mathbf{d} + H.c \tag{3.73}$$

$$\dot{\hat{\sigma}}^\dagger = i\omega_A\hat{\sigma}^\dagger + \frac{i}{\hbar}\hat{\mathbf{E}}_M^{(-)}(\mathbf{r}_A)\mathbf{d}\hat{\sigma}_z \tag{3.74}$$

$$\dot{\hat{\mathbf{f}}}(\mathbf{r},\omega) = -i\omega\hat{\mathbf{f}}(\mathbf{r},\omega) + \frac{\omega^2}{c^2}\sqrt{\frac{\varepsilon_I(\mathbf{r},\omega)}{\hbar\pi\varepsilon_0}}\mathbf{G}^*(\mathbf{r},\mathbf{r}_A,\omega)\mathbf{d}\hat{\sigma} \tag{3.75}$$

We must make a distinction between the radiation which is coupled to atom and the free radiation. The former is stemmed from a Rabi oscillating, radiating atomic dipole,

$$\hat{\mathbf{E}}_M^{(+)}(\mathbf{r},t) = \hat{\mathbf{E}}_{M,free}^{(+)}(\mathbf{r},t) + \frac{i}{\pi\varepsilon_0}\int_0^\infty d\omega\frac{\omega^2}{c^2}\mathrm{Im}\mathbf{G}(\mathbf{r},\mathbf{r}_A,\omega)\mathbf{d}\int_{t'}^{t} d\tau e^{-i\omega(t-\tau)}\hat{\sigma}(\tau) \tag{3.76}$$

Next step, we apply Markov approximation, we assume time integral runs over a small correlation time interval, $t - t' >> \tau_c$. If τ_c is negligible compared to the time scale atom is changing due to interaction with medium assisted field, then slowly varying quantity $\hat{\sigma}(\tau)e^{i\omega_A\tau)}$ can be taken out of time integral. By defining $\zeta(x) = \pi\delta(x) + i\wp x^{-1}$, we have,

$$\hat{\mathbf{E}}_M^{(+)}(\mathbf{r},t) = \hat{\mathbf{E}}_{M,free}^{(+)}(\mathbf{r},t) + \hat{\sigma}(t)\frac{i}{\pi\varepsilon_0}\int_0^\infty d\omega\frac{\omega^2}{c^2}\mathrm{Im}\mathbf{G}(\mathbf{r},\mathbf{r}_A,\omega)\mathbf{d}\zeta(\omega-\omega_A) \tag{3.77}$$

Pluging these results into our coupled integro-differential system, we obtain Langevin-type equations,

$$\dot{\hat{\sigma}}_z = -\gamma(1+\hat{\sigma}_z) + \left[\frac{2i}{\hbar}\hat{\sigma}^\dagger\hat{\mathbf{E}}_{M,free}^{(+)}(\mathbf{r}_A)\mathbf{d} + H.c\right] \tag{3.78}$$

$$\dot{\hat{\sigma}}^\dagger = \left[i(\omega_A - \delta\omega) - \tfrac{1}{2}\gamma\right]\hat{\sigma}^\dagger\frac{i}{\hbar}\hat{\mathbf{E}}_M^{(-)}(\mathbf{r}_A)\mathbf{d}\hat{\sigma}_z \tag{3.79}$$

In which, *gamma* corresponds to spontaneous emission rate, and $\delta\omega$ corresponds to Lamb-shift.

$$\gamma = \frac{2\pi}{\hbar^2}d_id_j\int_0^\infty d\omega\,\langle 0|\,\hat{E}_i(\mathbf{r}_A,\omega)\hat{E}_j^\dagger(\mathbf{r}_A,\omega_A)\,|0\rangle = \frac{2\omega_A^2 d_id_j}{\hbar\varepsilon_0c^2}\mathrm{Im}G_{ij}(\mathbf{r}_A,\mathbf{r}_A,\omega_A) \tag{3.80}$$

$$\delta\omega = \frac{d_id_j}{\hbar\pi\varepsilon_0}\wp\int_0^\infty \frac{\omega^2}{c^2}\frac{\mathrm{Im}G_{ij}(\mathbf{r}_A,\mathbf{r}_A,\omega)}{\omega-\omega_A} \tag{3.81}$$

The spontaneous emission is affected by surrounding medium by a factor known as *Purcell factor* $\sim \mathrm{Im}G_{ij}(\mathbf{r}_A, \mathbf{r}_A, \omega_A)$.

3.2.3 Harmonic Oscillator Approximation for Two-Level Atom

In order not to calculate all non-diagonal elements of Green's dyad and make Heisenberg equations of motion [38] [65] coupled, first order separable differential equations, we approximate our system as a harmonic oscillator. This approach is advantageous for systems involving initial photon pulses, as we will later see in the last chapter.

$$\hat{x} = \sqrt{\frac{\hbar}{2m\omega_A}}\left(\hat{b}^\dagger + \hat{b}\right) \tag{3.82}$$

$$\hat{p} = \sqrt{\frac{\hbar m\omega_A}{2}}\left(\hat{b}^\dagger - \hat{b}\right) \tag{3.83}$$

Combining them together, atomic Hamiltonian can be approximated to,

$$\hat{H}_A = \frac{\hat{p}^2}{2m} + \frac{1}{2}\omega_A\hat{x}^2 = \hbar\omega_A\hat{b}^\dagger\hat{b} \tag{3.84}$$

Relating position operator to the dipolar one, $\hat{\mathbf{d}} = q_{charge}\hat{x}\hat{\mathbf{e}}$ and defining coupling constant, $g = \frac{q_{charge}}{\hbar}\sqrt{\frac{\hbar}{2m\omega_A}}$, we get Jaynes-Cummings type interaction Hamiltonian,

$$\hat{H}_{int} = \hat{\mathbf{d}} \cdot\ \hat{\mathbf{E}}_M(\mathbf{r}_A) = -\hbar g\left(\hat{b}^\dagger\hat{\mathbf{e}}\cdot\hat{\mathbf{E}}_M^{(+)}(\mathbf{r}_A) + \hat{\mathbf{e}}\cdot\hat{\mathbf{E}}_M^{(-)}(\mathbf{r}_A)\hat{b}\right) \tag{3.85}$$

When harmonic oscillator approximation is used, Heisenberg equations of motion take the form,

$$\dot{\hat{\mathbf{f}}}(\mathbf{r},\omega) = -i\omega\hat{\mathbf{f}}(\mathbf{r},\omega) + ig\left[\hat{\mathbf{f}}(\mathbf{r},\omega), \hat{\mathbf{E}}_M^{(-)}(\mathbf{r}_A)\cdot\hat{\mathbf{e}}\right]\hat{b} \tag{3.86}$$

$$\dot{\hat{b}} = -i\omega_A\hat{b} + ig\hat{\mathbf{e}}\cdot\hat{\mathbf{E}}_M^{(+)}(\mathbf{r}_A) \tag{3.87}$$

Instead of making Markov approximation, now we will use Laplace transformations. At $t = 0$, we define $\hat{b}(t = 0)$ as $\hat{b}_0$ and $\hat{f}(\mathbf{r},\omega,t = 0)$ as $\hat{f}(\mathbf{r},\omega)$.

$$\hat{\mathbf{f}}(\mathbf{r},\omega,s) = \frac{1}{s+i\omega}\left(\hat{\mathbf{f}}(\mathbf{r},\omega) + ig\left[\hat{\mathbf{f}}(\mathbf{r},\omega), \hat{\mathbf{E}}_M^{(-)}(\mathbf{r}_A)\cdot\hat{\mathbf{e}}\right]\hat{b}(s)\right) \tag{3.88}$$

$$\hat{b}(s) = \frac{1}{s+i\omega_A}\left(\hat{b}_0 + ig\hat{\mathbf{e}}\cdot\hat{\mathbf{E}}_M^{(+)}(\mathbf{r}_A, s)\right) \tag{3.89}$$

Commutator in the equation has the form,

$$\left[\hat{f}_i(\mathbf{r},\omega), \hat{\mathbf{E}}_M^{(-)}(\mathbf{r}_A)\cdot\hat{\mathbf{e}}\right] = -i\sqrt{\hbar}\pi\varepsilon_0 \int_0^\infty d\omega' \int d^3\mathbf{r}' \sqrt{\varepsilon_I(\mathbf{r}',\omega')}\frac{\omega'^2}{c^2} G^*_{jk}(\mathbf{r}_A,\mathbf{r}',\omega') \tag{3.90}$$

$$\times \left[\hat{f}_i(\mathbf{r},\omega), \hat{f}^\dagger_k(\mathbf{r}',\omega')\right] e_j \tag{3.91}$$

$$= -i\sqrt{\frac{\hbar}{\pi\varepsilon_0}}\sqrt{\varepsilon_I(\mathbf{r},\omega)}\frac{\omega^2}{c^2} G^*_{ij}(\mathbf{r},\mathbf{r}_A,\omega) e_j \tag{3.92}$$

Inserting this commutator into equations of motions,

$$\hat{\mathbf{E}}_M(\mathbf{r},s) = \hat{\mathbf{E}}_{M,free}(\mathbf{r},s) + i\mathbf{M}(\mathbf{r},s)\hat{b}(s) \tag{3.93}$$

$$\hat{\mathbf{E}}_{M,free}(\mathbf{r},s) = \int_0^\infty \frac{d\omega}{s+i\omega}\hat{\mathbf{E}}_M(\mathbf{r},\omega) \tag{3.94}$$

$$\mathbf{M}(\mathbf{r},s) = \frac{\hbar g}{\pi\varepsilon_0}\int_0^\infty \frac{d\omega}{s+i\omega}\frac{\omega^2}{c^2}\mathrm{Im}\mathbf{G}(\mathbf{r},\mathbf{r}_A,\omega)\cdot\hat{\mathbf{e}} \tag{3.95}$$

Since $\hat{b}(t)$ is coupled to the electric field at position $\mathbf{r}_A$,

$$\hat{b}(s) = \frac{\hat{b}_0 + ig\hat{\mathbf{e}}\cdot\hat{\mathbf{E}}_{M,free}(\mathbf{r}_A,s)}{s + i\omega_A + g\hat{\mathbf{e}}\cdot\mathbf{M}(\mathbf{r}_A,s)} \tag{3.96}$$

$$\hat{E}_{M,i}(\mathbf{r},s) = \hat{E}_{M,i,\,free}(\mathbf{r},s) + i\mathbf{M}(\mathbf{r},s)\frac{\hat{b}_0 + ig\hat{\mathbf{e}}\cdot\hat{\mathbf{E}}_{M,free}(\mathbf{r}_A,s)}{s + i\omega_A + g\hat{\mathbf{e}}\cdot\mathbf{M}(\mathbf{r}_A,s)} \tag{3.97}$$

To further simplify this expression, we use lowest perturbation and Wigner-Weisskopf approximation, by changing $\mathbf{M}(\mathbf{r}_A,s)$ with $\mathbf{M}(\mathbf{r},-i\omega_A)$,

$$\gamma_{ij}(\mathbf{r},s) + i\delta_{ij}(\mathbf{r},s) = \frac{\hbar g^2}{\pi\varepsilon_0}\int_0^\infty \frac{d\omega}{s+i\omega}\frac{\omega^2}{c^2}\mathrm{Im}G_{ij}(\mathbf{r},\mathbf{r}_A,\omega) \tag{3.98}$$

$$\hat{b} = \frac{1}{s + i\omega'_A + \gamma}\left(\hat{b}_0 + ig\hat{\mathbf{e}}\cdot\hat{\mathbf{E}}_{M,free}(\mathbf{r}_A,s)\right) \tag{3.99}$$

$$\hat{E}_{M,i}(\mathbf{r},s) = \hat{E}_{M,i,\,free}(\mathbf{r},s) + \frac{i}{g}\left(\Gamma_{ij}(\mathbf{r},s) + i\delta_{ij}(\mathbf{r},s)\right)\hat{e}_j\hat{b}(s) \tag{3.100}$$

Where, the new forms of spontaneous emission rate, γ, and, Lamb-shift, $\delta\omega$ are,

$$\delta\omega_A = \omega'_A - \omega_A = g^2\frac{\hbar}{\pi\varepsilon_0}\mathrm{Im}\left[\int_0^\infty \frac{d\omega}{i(\omega-\omega_A)}\mathbf{e}\cdot\mathrm{Im}\mathbf{G}(\mathbf{r}_A,\mathbf{r}_A,\omega)\cdot\mathbf{e}\right] \tag{3.101}$$

$$\gamma = g^2\frac{\hbar}{\pi\varepsilon_0}\mathrm{Re}\left[\int_0^\infty \frac{d\omega}{i(\omega-\omega_A)}\mathbf{e}\cdot\mathrm{Im}\mathbf{G}(\mathbf{r}_A,\mathbf{r}_A,\omega)\cdot\mathbf{e}\right] \tag{3.102}$$

Note that the expression for Lamb-shift is not converging, and needs to be renormalized. This is often done by means of double Lorentzian smearing functions of the form, $\mathcal{S}(\mathbf{x}) = \omega/(\pi^2(r^2+\omega^2)^2)$, or just by Gaussians centered at atomic frequency and position.

Chapter 4

SINGLE PHOTON EXCITATION IN L-HMM

Excitation of an atom by a single photon pulse has applications in quantum information science [66], quantum imaging and subdiffraction imaging. Processes involving single photons often involves spontaneously emitting atoms or quantum dots. When all atomic and radiation degrees of freedom are taken into account, spontaneous emission [38] [65] can be considered as a unitary process, so in principle it can be reversed in time. A perfect time-reversal of a spontaneously emitted single photon pulse, which should mimick the pulse shape in time and space, could excite an atom with certainty.

In free space, there is perfect spherical symmetry. Thus, a time reversal of a spontaneously emitted single photon pulse would require swapping whole solid angle, which is practically not possible. On the other hand, if the symmetry of the system is somehow broken such that power is flowing directionally, then a directional single photon pulse can be designated. Choquette et. al [38] used an atom sitting on top of a metal layer in Kretschmann configuration, see Fig. 4.1 4.2. They made use of directionality imposed by surface plasmon excitation angle, which results of a cone with half angle θ_{SP}. They generated their own conical single photon pulse, which is more or less time reversal of spontaneously emitted photon. By following Choquette et.al's [] footsteps and using extreme anisotropy present in layered Hyperbolic Metamaterials, we propose using a conical single photon pulse to match the resonance cone, θ_{RC} of l-HMM. We first provide theoretical background for a photon pulse in a specific mode.

4.1 Specific Single-Photon Mode

If we omit non-resonant processes for atoms and molecules that are excited by just a single photon, we can use harmonic oscillator approximation developed in last chapter. Since we are only interested in resonant processes at specific frequencies, i.e designing pulses with

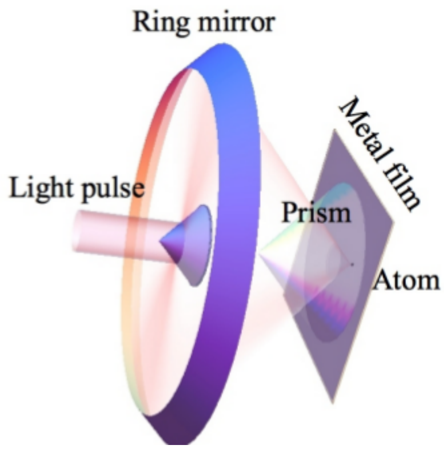

Figure 4.1: The system proposed by Choquette et al [65] to emulate time-reversal of an atom spontaneously emitting single photon in Kretschmann configuration. Conical lens creates conical field similar to one diverted by prism.

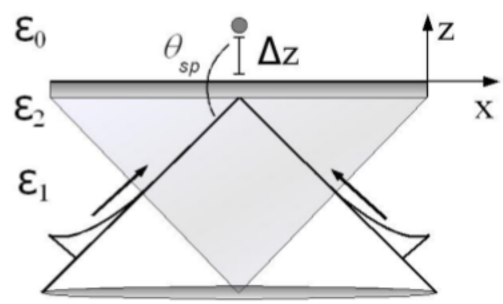

Figure 4.2: 2D Cross section of the system proposed by Choquette et al [65] to emulate time-reversal of an atom spontaneously emitting single photon in Kretschmann configuration. Conical lens creates conical field similar to one diverted by prism.

very narrow frequency widths, we will not need permittivity information for all frequencies.

We follow Choquette et. al's proposal[65], in which, they start with mode annihilation operators, $\hat{a}$, that annihilates a photon into a specific field mode, $\mathcal{E}(\mathbf{r})$.

Vacuum field amplitude of a single photon state in this mode, $|\psi\rangle = \hat{a}^\dagger |vac\rangle$, is just,

$$\mathcal{E}(\mathbf{r}) = \langle vac| \hat{\mathbf{E}}(\mathbf{r}) |\psi\rangle \tag{4.1}$$

The annihilation operator of this specific mode is,

$$\hat{a} = \frac{2\varepsilon_0\epsilon_\infty}{\hbar}\int d^3\mathbf{r}\int_0^\infty \frac{d\omega}{\omega}\mathcal{E}^*(\mathbf{r})\cdot\hat{\mathbf{E}}(\mathbf{r},\omega) \tag{4.2}$$

Where $\epsilon_\infty = \lim_{|\omega|\to\infty}\varepsilon(\mathbf{r},\omega)$. To check consistency of the expression for mode annihilation operator, we check electric field amplitude of a single photon state in this specific mode,

$$\langle vac|\,\hat{\mathbf{E}}(\mathbf{r})\hat{a}^\dagger\,|vac\rangle = \left[\hat{\mathbf{E}}(\mathbf{r}),\hat{a}^\dagger\right] \tag{4.3}$$

$$= \frac{2\epsilon_\infty}{\pi}\int d^3\mathbf{r}'\mathcal{E}_j(\mathbf{r}')\int_0^\infty d\omega\frac{\omega}{c^2}\mathrm{Im}G_{ij}(\mathbf{r},\mathbf{r}',\omega) \tag{4.4}$$

Where the integral can be found using these properties of classical Green's tensors,

$$\int_0^\infty d\omega\frac{\omega}{c^2}\mathrm{Im}G_{ik}(\mathbf{r},\mathbf{r}',\omega) = \frac{1}{2ic^2}\int_{-\infty}^\infty d\omega\omega G_{ik} = \frac{\pi}{2\epsilon_\infty}\delta_{ik}\delta(\mathbf{r}-\mathbf{r}') \tag{4.5}$$

$$\lim_{|\omega|\to\infty}q^2(\mathbf{r},\omega)G_{ik}(\mathbf{r},\mathbf{r}',\omega) = -\delta_{ik}\delta(\mathbf{r}-\mathbf{r}') \tag{4.6}$$

with $q(\mathbf{r},\omega) = \sqrt{\varepsilon}\frac{w}{c}$, electric field amplitude is validated

$$\langle vac|\,\hat{\mathbf{E}}_i(\mathbf{r})\hat{a}^\dagger\,|vac\rangle = \int d^3x\mathcal{E}_k(\mathbf{x})\delta_{ik}\delta(\mathbf{r}-\mathbf{x}) = \mathcal{E}_i(\mathbf{r}) \tag{4.7}$$

Meanwhile, commutation relations for this specific field mode must alse be met,

$$\left[\hat{a},\hat{a}^\dagger\right] = \frac{4\varepsilon_0\epsilon_\infty^2}{\hbar\pi c^2}\int d^3r\int d^3r'\mathcal{E}_i^*(\mathbf{r})\mathcal{E}_j(\mathbf{r})\int_0^\infty d\omega\mathrm{Im}G_{ij}(\mathbf{r},\mathbf{r}',\omega) = 1 \tag{4.8}$$

4.2 Time-Inverted Single Photon Pulse For Atomic Excitation

To find single-photon excitation probability, $P_e(t)$, we should first create a field mode ansatz to mimick time-reversal of a spontaneously emitted light. Again, following Choquette et al's proposal [65] of field ansatz in momentum space, which is a perfect approximation for an exact cone,

$$\mathcal{E}(\mathbf{k}) = \left(\mathbf{e}-\mathbf{k}\frac{\mathbf{e}\cdot\mathbf{k}}{k^2}\right)\mathcal{A} \tag{4.9}$$

$$\tag{4.10}$$

The field ansatz, $\mathcal{E}(\mathbf{k})$ has three major components. The term $\left(\mathbf{e} - \mathbf{k}\frac{\mathbf{e}\cdot\mathbf{k}}{k^2}\right)$ ensures that the time-reversed field remains transverse and produces the same field profile as an electric dipole pointing $\hat{e}$ direction.

$$\mathcal{A} = \mathcal{N}\frac{e^{i\omega_k t_{\mathcal{E}} - i\mathbf{k}\cdot\mathbf{r}_{\mathcal{E}}}}{-i(\omega_A - \omega_k) + \gamma_{\mathcal{E}}}h(\theta) \tag{4.11}$$

The amplitude part, $\mathcal{A}$ has four components. First, $\mathcal{N}$ ensures normalization. Second, Denominator is a Lorentzian centered in Lamb-shifted atomic frequency, $\delta\omega'$. This factor is also responsible for field enhancement as distance from the origin increases. Third, exponential factor, $e^{i\omega_k t_E - i\mathbf{k}\cdot\mathbf{r}_{\mathcal{E}}}$, guarantees the pulse is propagating towards the origin (incoming). $t_\varepsilon >> \gamma^{-1}$ is the time when the pulse is reverted in time such that it cuts the field at $r = ct_\varepsilon\sqrt{\epsilon_\parallel}$. r_ε is the focal point of the field in vacuum, which can be used to optimize P_e .

$$h(\theta) = exp\left\{-\frac{(\theta - \theta_{RC})^2}{\delta\theta^2}\right\} \tag{4.12}$$

Last, the right most part, $h(\theta)$, provides the geometry of the pulse. Since it is a Gaussian envelope, it contains the pulse within a small range, $\delta\theta$ of inclination angles, $\theta = cos^{-1}\left(\frac{k_z}{k}\right)$, centered around resonance cone angle, θ_{RC}. With the addition of this envelope, keeping the pulse conical, this field ansatz could effectively simulate the time reversal of an electrical dipole embedded in a HMM. Choquette et. al [65] proposed this ansatz to be centered in surface plasmon excitation angle, θ_{SP}, for a multilayered system (Kreschmann configuration: vacuum, dielectric prism, metal surface), which has similiar field outcome.

Once we constructed this field mode, the probability of transfering this excitation into atomic mode, i.e single photon excitation probability, can be calculated by means of time dependent perturbation theory. If we start with the initial state, $|\psi_0\rangle = \hat{a}^\dagger |vac\rangle \otimes |0\rangle$, which contains single photon excitation in the designated field mode, and, as a target state, want to end up in the excited atomic state, $|\psi_{target}\rangle = \hat{b}^\dagger |vac\rangle \otimes |0\rangle$, the first order perturbation will give excitation probability:

$$P_e(t) = |\langle 0|\, \hat{b}(t)\, |\psi_0\rangle|^2 \tag{4.13}$$

$$= |\left[\hat{b}(t), \hat{a}^\dagger\right]|^2 \tag{4.14}$$

4.3 Excitation Probability Inside Uniaxial Medium

$$P_e(t) = |\left[\hat{b}(t), \hat{a}^\dagger\right]|^2 \tag{4.15}$$

To evaluate this commutator, we need to make a Laplace transform, as we did in last sections. It is clearly easier than solving coupled differential equations for atom coupled to polaritonic continuum, involving non-diagonal elements of Green's tensor.

$$\left[\hat{b}(t), \hat{a}^\dagger\right] = \frac{1}{2\pi i} \int_{\epsilon - i\infty}^{\epsilon + i\infty} ds e^{ts} \left[\hat{b}(s), \hat{a}^\dagger\right] \tag{4.16}$$

$$= \frac{g\epsilon_\infty}{\pi^2} \int_{\epsilon - i\infty}^{\epsilon + i\infty} ds e^{ts} \frac{\mathbf{e}_k}{s + i\omega_A' + \gamma} \int_0^\infty \frac{d\omega}{s + i\omega} \int d^3 r \mathcal{E}_i(\mathbf{r}) \frac{\omega}{c^2} \mathrm{Im} G_{ki}(\mathbf{r}_A, \mathbf{r}, \omega) \tag{4.17}$$

This Cauchy integral has contributions from poles $s = -i\omega$ and $s = -i\omega_A' - \gamma$. If the time period to excite the atom using single photon exceeds the time period for the day in many orders of magnitude,$t >> \gamma^{-1}$, the contribution from second pole is suppressed. In this case, only the first pole, $s = -i\omega$, is relevant:

$$\left[\hat{b}(t), \hat{a}^\dagger\right] = \frac{2g\epsilon_\infty}{\pi} \int_0^\infty d\omega \frac{e^{-i\omega t}}{\omega - \omega_A' + i\gamma} \frac{\omega}{c^2} \int d^3 x \hat{\mathbf{e}} \cdot \mathrm{Im} \mathbf{G}(\mathbf{r}_A, \mathbf{x}, \omega) \mathcal{E}(\mathbf{x}) \tag{4.18}$$

To evaluate three dimensional Fourier transform further, we should use parameters in the system geometry. In our system, the atom to be excited is positioned at the origin, $\mathbf{r}_A = (0, 0, 0)$, and single-photon pulse coming from below, $(z < 0)$, to $z_A = 0$. Since the HMM geometry we use is a stack of metal-dielectric layers, leading to uniaxial electromagnetic response, in other words, our geometry possessing azimuthal (cylindrical) symmetry, we can make use of two dimensional Fourier transforms around atomic positions. This corresponds to Weyl representation of a spherical wave by planewaves, which is mostly used in Fourier optics when a symmetry is present:

$$\mathbf{G}(\mathbf{r}_A, \mathbf{x}, \omega) = \int \frac{d^2 q_\parallel}{2\pi} e^{iq_\parallel \cdot (\mathbf{r}_A - \mathbf{x})} \mathbf{G}(\mathbf{q}_\parallel, \omega, z_A, z) \tag{4.19}$$

Having Fourier transformed our Green's tensor in 2D, we obtained an identity mapping the fields for certain transverse values of wavevector and certain vertical positions (z-axis) into atomic position. Because of the symmetry, change of field in vertical positions only corresponds to a phase difference:

$$\mathbf{G}(\mathbf{q}_\parallel, \omega, z_A, z) = e^{-(i\mathrm{sign}[z - z_A])\beta z} \mathbf{G}(\mathbf{q}_\parallel, \omega, z_A) \tag{4.20}$$

We were able to take phase part out of the integral, which depends on the wavevector in the vertical direction, β,

$$\beta = \left((\frac{\omega}{c} \sqrt{\varepsilon_\parallel} \right)_z = \left[\varepsilon_\parallel \frac{\omega^2}{c^2} - \mathbf{q}_\parallel^2 \right]^{\frac{1}{2}} \tag{4.21}$$

$$(i\mathrm{sign}[z - z_A])\beta z = -i \left(\frac{\omega}{c} \sqrt{\varepsilon_\parallel} \right)_z \tag{4.22}$$

Where the dyadic expression involving transverse wavevectors and atomic position is nothing but one dimensional inverse Fourier transform in vertical direction, with respect to atomic position:

$$\mathbf{G}(\mathbf{q}_\parallel, \omega, z_A) = \int \frac{dq_z}{\sqrt{2\pi}} e^{iq(z_A - z)} \mathbf{G}(\mathbf{q}, \omega) \tag{4.23}$$

Once we plug all these expressions into commutator, we have,

$$\left[\hat{b}(t), \hat{a}^\dagger \right] = \frac{ig\epsilon_\infty}{\pi} \int_0^\infty d\omega \frac{e^{-i\omega t}}{\omega - \omega'_A + i\gamma} \frac{\omega}{c^2} \int d^2 q_\parallel \int_{-\infty}^{\infty} dz \hat{\mathbf{e}} \cdot \tag{4.24}$$

$$\times \left(e^{i\mathbf{q}_\parallel e^{-i\beta z} \cdot \mathbf{r}_A} \mathbf{G}(\mathbf{q}_\parallel, \omega, z_A) \cdot \mathcal{E}(\mathbf{q}_\parallel, z) - e^{-i\mathbf{q}_\parallel \cdot \mathbf{r}_A} e^{i\beta z} \mathbf{G}^*(\mathbf{q}_\parallel, \omega, z_A) \cdot \mathcal{E}(-\mathbf{q}_\parallel, z) \right) \tag{4.25}$$

$$= ig\epsilon_\infty \sqrt{\frac{2}{\pi}} \int_0^\infty d\omega \frac{e^{-i\omega t}}{\omega - \omega'_A + i\gamma} \frac{\omega}{c^2} \int d^2 q_\parallel e^{i\mathbf{q}_\parallel \cdot \mathbf{r}_A} \hat{\mathbf{e}} \cdot \tag{4.26}$$

$$\times \left(\mathbf{G}(\mathbf{q}_\parallel, \omega, z_A) \cdot \mathcal{E}(\mathbf{q}_\parallel, +\beta) - \mathbf{G}^*(\mathbf{q}_\parallel, \omega, z_A) \cdot \mathcal{E}(-\mathbf{q}_\parallel, -\beta) \right) \tag{4.27}$$

Since the pulse is coming from $(z < 0)$, only $q_z = \beta > 0$ components survive. Because of $\left(\hat{\mathbf{e}}_{dip} - \frac{\hat{\mathbf{e}}_{dip}\cdot\mathbf{q}}{q^2}\mathbf{q}\right)$ factor, which guarantees transversity of time-inverted, conical, spontaneously emitted single-photon pulse, and, azimuthal symmetry; only $\mathbf{G}_{33}(\mathbf{q}, \omega, z_A)$ term survives for $\hat{\mathbf{e}}_{dip} = \hat{z}$ corresponding to $E_z \neq 0$ TM-mode, and, $G_{22}(\mathbf{q}, \omega, z_A)$ for $\hat{\mathbf{e}}_{dip} = \hat{y}$ corresponding to $E_y \neq 0$ TE-mode.

⋇ For $\hat{\mathbf{e}} = \hat{z}$, and using the spherical coordinates for 2D Fourier transform $d^2q_{\parallel} = qsin(\theta)dqd\phi$:

$$\left[\hat{b}(t), \hat{a}^{\dagger}\right] = i\sqrt{\frac{2}{\pi}}g\epsilon_{\infty}\left(-cos(2\theta)sin(\theta)\right)e^{-\frac{(\theta-\theta_{RC})^2}{\delta\theta^2}}\int\limits_{0}^{\infty}d\omega\frac{e^{-i\omega t+i\omega_{\mathcal{E}}t_{\mathcal{E}}}}{\omega-\omega'_A+i\gamma}\frac{\omega}{c^2} \tag{4.28}$$

$$\times\int\limits_{0}^{\infty}dq\frac{e^{iq(r_A sin\theta - r_{\mathcal{E}})}}{-i(\omega'_A-\omega)+\gamma}\int\limits_{0}^{2\pi}d\phi\mathbf{G}_{33}(\mathbf{q}_{\parallel}, \omega, z_A) \tag{4.29}$$

Defining $\alpha = \left(\epsilon_{\parallel} - \epsilon_{\perp}\right)cos2\theta - \left(\epsilon_{\parallel} + \epsilon_{\perp}\right)$, setting $c = 1$, $\eta = \sqrt{\frac{\epsilon_{\parallel}\epsilon_{\perp}}{\alpha}}$ and $t_{\mathcal{E}} = r_{\mathcal{E}}\sqrt{\epsilon_{\parallel}}$, for the pole $\omega = \omega_A - i\gamma$ our expression becomes:

$$\left[\hat{b}(t), \hat{a}^{\dagger}\right] = 16\sqrt{2}\pi^{\frac{7}{2}}g\epsilon_{\infty}sin\theta cos\theta e^{-\frac{(\theta-\theta_{RC})^2}{\delta\theta^2}}\left(\omega_A - i\gamma\right)\right)e^{-i(\omega_A-\gamma)r_{\varepsilon}\sqrt{\epsilon_{\parallel}}} \tag{4.30}$$

$$\times\Bigg\{-i\frac{e^{-i\sqrt{\epsilon_{\parallel}}(\omega_A-i\gamma)r_{\varepsilon}cos\theta}}{\sqrt{\epsilon_{\parallel}}\left[\gamma+i\left((\omega_A-i\gamma)\sqrt{\epsilon_{\parallel}}-\omega_A\right)\right]} \tag{4.31}$$

$$+\frac{\left(1-\epsilon_{\parallel}^2\epsilon_{\perp}\right)e^{-\sqrt{2}(\omega_A-i\gamma)r_{\varepsilon}cos\theta\eta}\sqrt{\pi}\left[-(\gamma-i\omega_A)\alpha+(\omega_A-i\gamma)\sqrt{2\alpha\epsilon_{\parallel}\epsilon_{\perp}}\right]}{\sqrt{\epsilon_{\parallel}\epsilon_{\perp}\alpha}\left[\epsilon_{\parallel}\left(2\epsilon_{\perp}(\omega_A-i\gamma)^2+(\gamma-i\omega_A)^2\right)+\epsilon_{\perp}(\gamma-i\omega_A)^2-(\epsilon_{\parallel}-\epsilon_{\perp})(\gamma-i\omega_A^2)cos2\theta\right]}\Bigg\} \tag{4.32}$$

⋇ For $\hat{\mathbf{e}} = \hat{y}$,

$$\left[\hat{b}(t), \hat{a}^{\dagger}\right] = ig\epsilon_{\infty} sin^2\theta e^{-\frac{(\theta-\theta_{RC})^2}{\delta\theta^2}} \int_0^{\infty} d\omega \frac{e^{-i\omega t + i\omega_{\mathcal{E}} t_{\mathcal{E}}}}{\omega - \omega'_A + i\gamma} \frac{\omega}{c^2} \tag{4.33}$$

$$\times \int_0^{\infty} dq \frac{e^{iq(r_A sin\theta - r_{\mathcal{E}})}}{-i(\omega'_A - \omega) + \gamma} \int_0^{2\pi} d\phi \mathbf{G}_{22}(\mathbf{q}_{\|}, \omega, z_A) sin^2\phi \tag{4.34}$$

for the pole $\omega = \omega_A - i\gamma$ our expression becomes:

$$\left[\hat{b}(t), \hat{a}^{\dagger}\right] = 8\sqrt{2}\pi^4 g\epsilon_{\infty} sin^2\theta e^{-\frac{(\theta-\theta_{RC})^2}{\delta\theta^2}} \sqrt{\epsilon_{\|}\epsilon_{\perp}} \left(\omega_A - i\gamma\right)\right) e^{-i(\omega_A-\gamma) r_{\varepsilon}\sqrt{\epsilon_{\|}}} e^{-\sqrt{2}(\omega_A - i\gamma) r_{\varepsilon} cos\theta\eta} \tag{4.35}$$

$$\times \frac{\left[-(\gamma - i\omega_A)\alpha + (\omega_A - i\gamma)\sqrt{2\alpha\epsilon_{\|}\epsilon_{\perp}}\right] \left(\epsilon_{\|}\epsilon_{\perp} cos^2\theta - \epsilon_{\perp} sin^2\theta\right)}{\sqrt{\alpha}\left[\epsilon_{\|}\left(2\epsilon_{\perp}(\omega_A - i\gamma)^2 + (\gamma - i\omega_A)^2\right) + \epsilon_{\perp}(\gamma - i\omega_A)^2 - (\epsilon_{\|} - \epsilon_{\perp})(\gamma - i\omega_A^2) cos2\theta\right]} \tag{4.36}$$

We first start by checking the validity of these expressions. By following the footsteps of Choquette et al [38], in order our field ansatz to mimic a conical field, restricted by half-cone angle θ_{res} inside uniaxial medium, it should be able to imitate atomic dipole emission in vacuum. Spontaneous emission in vacuum, which has a spatial field profile close to dipolar emission, is not directional. In order our expressions to be valid, once the medium is set to vacuum, $\epsilon_{\|} = \epsilon_{\perp} = 1$, and cone angle is brought to 2π in the so-called "spherical wave limit", single photon excitation probability should converge to unity. Our calculations, demonstrated in Figure 4.4, verify this claim. Creating a non-directional single photon pulse terminating at a certain atomic position, which is the time-reversal of spontaneously emitted photon in vacuum, is not physically feasible, yet works as a good, theoretical test case.

Once verified, we set medium parameters to Type 1 HMM, Type 2 HMM and positive uniaxial cases, where $\epsilon_{\|} = \pm 4.3 + 0.4i$ and $\epsilon_{\perp} = \mp 11 + 1j * 0.07$ leading $\theta_{RC} = \arctan\left(\left|(\epsilon_{\|}/\epsilon_{\perp})\right|\right)$, which is around 21.35 degrees for our setting. In the case of atom embedded in Type 1 HMM, and dipole pointing in z direction (see Figure 4.5), we see single photon excitation probabilities upto 0.8, for decay rate $\gamma = 6\gamma_0$, which can be manipulated

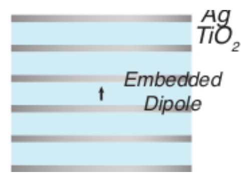

Figure 4.3: The system proposed by Cortez et al [65], where dipole embedded in HMM, which is made out of Ag, and, TiO_2 layers of 10 nm and 30 nm thickness. Their model indicates that at $\lambda = 900$ nm, dielectric tensor yields "$-4.3 + 0.02i$" in transverse, and "$11 + 0.04i$" in longitudinal direction, according to Effective Medium Theory.

by Purcell factor engineering in the media, then a gradual decrease. These high probabilities can be attributed to spatial overlap between time-reversed field, and conical field output by dipole in Figure 2.12. When dipole is pointing in y direction (see Figure 4.8), no high probability is observed due to small spatial overlap with field in 2.14. These are also the cases for both alignments in Type 2 HMM, as demonstrated in figures 4.9 4.6, because of the "butterfly" spatial field profile in figures 2.15 2.13. In positive uniaxial media, where both medium parameters are greater than zero, $\epsilon_{||} > 0$ and $\epsilon_{\perp} > 0$, relatively high probabilities observed (see figures 4.10 4.7).

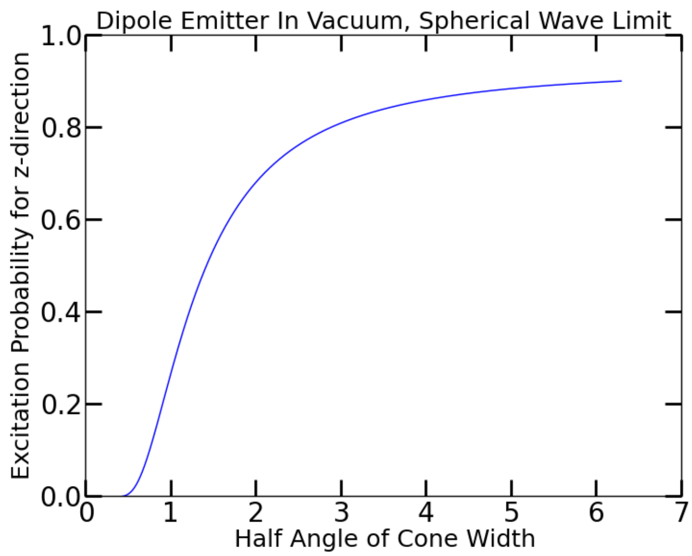

Figure 4.4: To check validity of our expressions, half-cone angle θ, is set to "spherical wave limit", 2π, such that excitation probability goes to unity. This is the perfect time-reversal of a spontaneously emitting atomic dipole in vacuum.

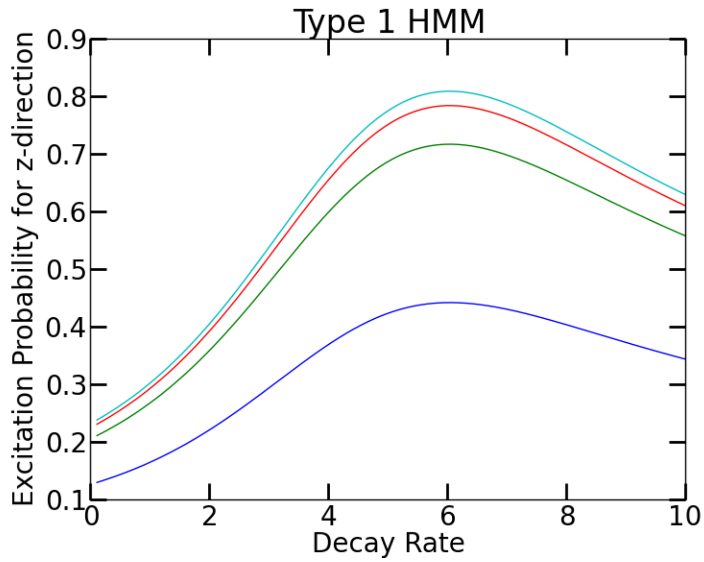

Figure 4.5: Single Photon Excitation inside Type 1 HMM where $\epsilon_{\parallel} = 4.3 + 0.4i$ and $\epsilon_{\perp} = -11 + 0.07i$ for the case of dipole pointing in $\hat{\mathbf{e}} = \hat{z}$ direction. Different colours representing different cone half-angles

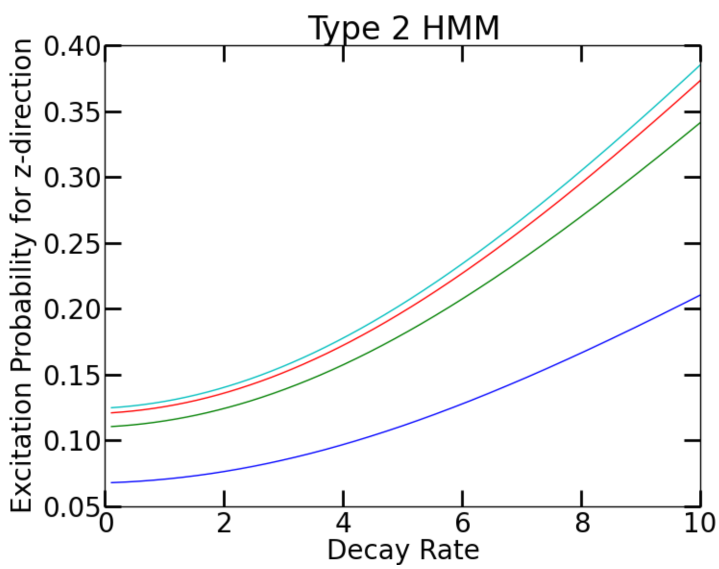

Figure 4.6: Single Photon Excitation inside Type 2 HMM where $\epsilon_{\parallel} = -4.3 + 0.4i$ and $\epsilon_{\perp} = 11 + 0.07i$ for the case of dipole pointing in $\hat{\mathbf{e}} = \hat{z}$ direction. Different colours representing different cone half-angles

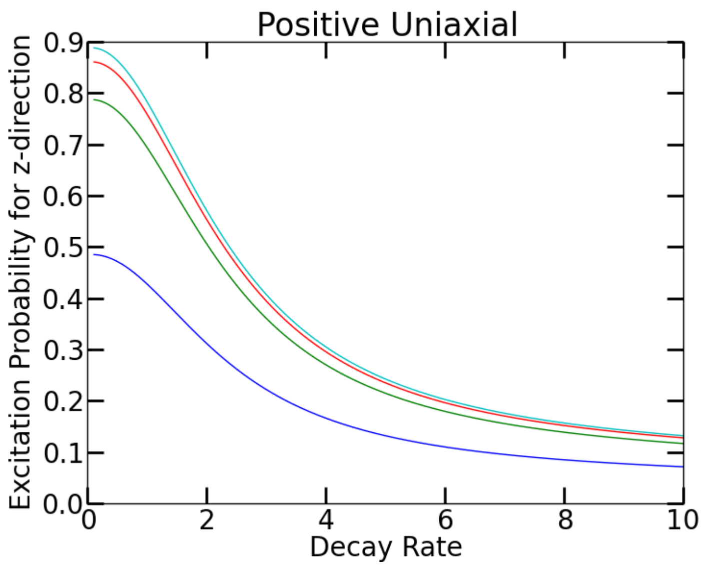

Figure 4.7: Single Photon Excitation inside Positive Uniaxial Material where $\epsilon_{\parallel} = 4.3+0.4i$ and $\epsilon_{\perp} = 11 + 0.07i$ for the case of dipole pointing in $\hat{\mathbf{e}} = \hat{z}$ direction. Different colours representing different cone half-angles

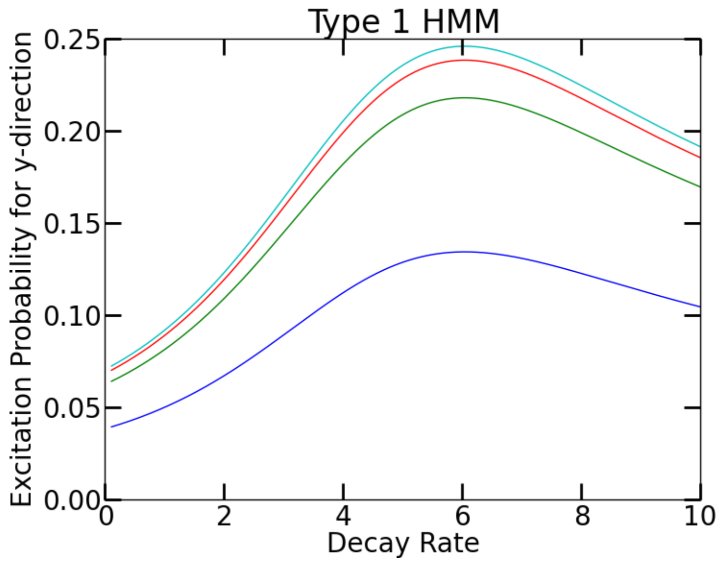

Figure 4.8: Single Photon Excitation inside Type 1 HMM where $\epsilon_{\parallel} = 4.3 + 0.4i$ and $\epsilon_{\perp} = -11 + 0.07i$ for the case of dipole pointing in $\hat{\mathbf{e}} = \hat{y}$ direction. Different colours representing different cone half-angles

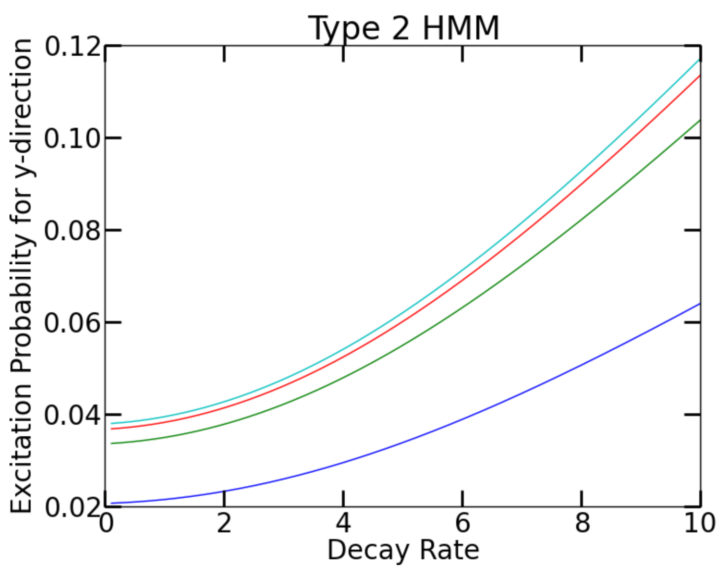

Figure 4.9: Single Photon Excitation inside Type 2 HMM where $\epsilon_{\parallel} = -4.3 + 0.4i$ and $\epsilon_{\perp} = 11 + 0.07i$ for the case of dipole pointing in $\hat{\mathbf{e}} = \hat{y}$ direction. Different colours representing different cone half-angles

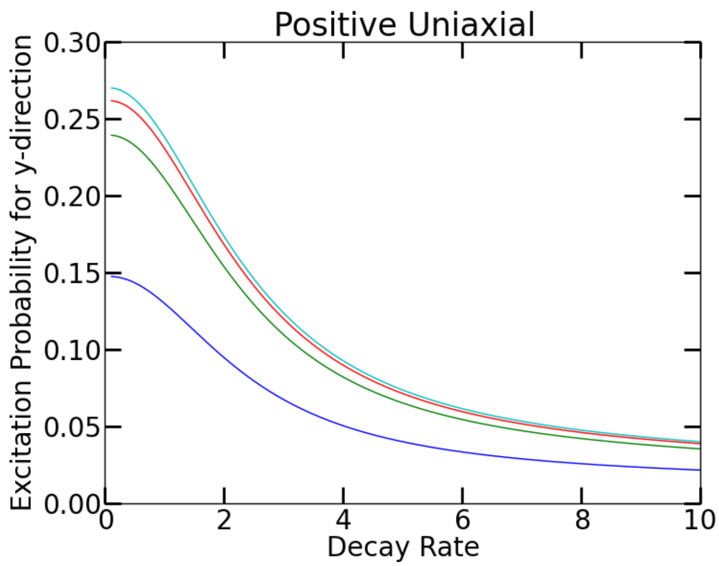

Figure 4.10: Single Photon Excitation inside Positive Uniaxial Material where $\epsilon_{\parallel} = 4.3 + 0.4i$ and $\epsilon_{\perp} = 11 + 0.07i$ for the case of dipole pointing in $\hat{\mathbf{e}} = \hat{y}$ direction. Different colours representing different cone half-angles

Chapter 5

CONCLUSIONS

Hyperbolic metamaterials are popular because of the presence of high-k states that could be harnessed for sub-diffraction imaging [31], and, high Purcell factors for single photon sources [32] [34] . Both of these properties can be combined for the sake of quantum information processing and quantum imaging (e.g, to enhance the proposal of Thiel [3]). To do so, we needed theoretical foundations of classical and quantum electrodynamics inside complex media. The Green's tensor formalism, although is not the only way of examining such systems, was preferred throughout the thesis, because it is a compact, self-consistent theory and does not refer to any microscopic model. Also, the dyads computed for classical problems (e.g, by a commercial FDTD simulator) can be used to solve quantum mechanical problems.

Being motivated by the heuristic that time reversal symmetry of a physical system that is particularly good at a certain task, such as an atom spontaneously emitting single photons inside a medium with high Purcell factor, should be able to deliver the reverse of this task again with the good efficiency, we applied this formalism to calculate the single photon excitation probability of an atom embedded in l-HMM. Although we had promising results, there is still no known way of implementing the system we proposed, because outcoupling light into HMM is still an issue [50] [34], hitherto obscuring the dream of making a hyperlens.

As a future work, on the other hand, instead of embedding a dipole inside a l-HMM, the atom in question or an array of atoms can be suspended on top of a l-HMM, as proposed by [67]. Some quantum information tasks such as entanglement transfer is shown [22] [17] [19] to be very efficient in similar systems, like plasmonic waveguides. Entanglement transfer and similar quantum information tasks for atoms suspended over l-HMM will be examined in the future.

Chapter 6

APPENDIX

6.1 Equivalence of Classical-Quantum Modes and Their Relation to Green's Dyad

The most basic form of the electric field operator, which we can further generalize to more complex ones by superposing with similar structures, is given, in the Heisenberg picture, as follows [42]:

$$\hat{\mathbf{E}} = \sum_k \left(\mathbf{E}_k^+ \hat{a}(t) + \mathbf{E}_k^- \hat{a}^\dagger(t) \right) \tag{6.1}$$

The complex field $\mathbf{E}_k^+$ ($\mathbf{E}_k^-$) corresponds to the field envelope of positive (negative) frequency. For the free fields not interacting with atoms, equation of motions for bosonic operators are given by Heisenberg time-evolution operators of the unperturbed Hamiltonians, leading harmonic time dependence, $\hat{a}(t) = \hat{a}(0)e^{-i\omega t}$ ($\hat{a}^\dagger(t) = \hat{a}^\dagger(0)e^{i\omega t}$). These (counter) rotating complex fields are comprised of normal modes, $\mathbf{E}_k^\pm = \sqrt{\frac{\hbar\omega_k}{2\varepsilon_0}}\mathbf{u}_k^{(*)}$.

Quasi-classical normal mode functions (classical fields with quantization volumes), which satisfy homogeneous wave equation and assumes their specific forms due to boundary conditions, have complex vectoral (3 x 1) form, and they carry the information regarding spatial spread, geometry, polarization, direction, wave envelope and orbital angular momentum [**?**] of the field; anything, but amplitude and quantum statistics information carried in bosonic operators, and states (especially coherence, interference of different modes and superposition). The normal mode function [**?**][**?**][15] of a cavity with perfectly conducting walls (PC), a cavity with periodical boundary conditions (PB), a surface plasmon polariton emitted by a single SPP source (SPP), and electric field operator of the superposition of

Laguerre-Gaussian normal modes, v_{10}, v_{01} lying on waist plane are as follows,

$$\mathbf{u}_{k\lambda}^{PC} = \frac{1}{V_{quantize}} sin(k_x x) sin(k_y y) sin(k_z z)\epsilon_{k\lambda} \tag{6.2}$$

$$\mathbf{u}_{k\lambda}^{PB} = \frac{1}{V_{quantize}} e^{ikr}\epsilon_{k\lambda} \tag{6.3}$$

$$\mathbf{u}_{k\lambda}^{SPP} = \frac{1}{V_{quantize}} e^{-\kappa_j z}\left(\hat{\mathbf{K}} - i\frac{K}{\kappa_j}\hat{\mathbf{z}} exp(i\hat{\mathbf{K}}\mathbf{R}\right) \tag{6.4}$$

$$\hat{\mathbf{E}} = v_{10}(x,y)\hat{b}_+ + v_{01}\hat{b}_- \tag{6.5}$$

These normal mode functions are inherently connected to density of modes [38] or photonic density of states, $\rho_\mu(r_0, \omega_0)$.Presence of this photonic mode density modifies [42] the ratio of average power radiated by a classical harmonic oscillator, such as dipolar antenna, inside a dispersing/absorbing media to the one in free space, and equivalently, the ratio of spontaneous emission by a quantum dipolar source (atoms, q.dots etc.) in media to the one in free space, also known as Purcell factor. Then, Novotny [42] shows the equivalence of Green's tensor formalism by expanding the field in terms of modes and amplitudes in Helmholtz equation,

$$\frac{P}{P_0} = \frac{\gamma}{\gamma_0} = \frac{2\Pi c^3}{\omega^3}\rho_\mu(r_0, \omega_0) \tag{6.6}$$

$$\rho_\mu(r_0, \omega_0) = 3\sum_k [\mathbf{n}_\mu \cdot (\mathbf{u}_k \otimes \mathbf{u}_k^*) \cdot \mathbf{n}_\mu] \tag{6.7}$$

$$\mathbf{G}(r, r_0; w) = \sum_k c^2 \frac{\mathbf{u}_k^*(r', \omega_k) \otimes \mathbf{u}_k(r, \omega_k)}{\omega_k^2 - \omega^2} \tag{6.8}$$

$$\rho(r_0, \omega_0) = \sum_\mu^3 \rho_\mu(r_0, \omega_0) = \frac{6\omega_0}{\pi c^2} Tr\left[Im\left[\mathbf{G}(r_0, r_0; w_0)\right]\right] \tag{6.9}$$

Tame et al [15] use these properties of normal modes to quantize SPPs, hence showing equivalence of this formalism to Green's tensor formalism devised by Knoll et al [37]. Starting by discretization of classical mode function, $\mathbf{u}_{k\lambda}^{SPP}$, and amplitudes, keeping dispersion relations $K = (\omega/c)\sqrt{\varepsilon(\omega)/(\varepsilon(\omega)+1)}$, $\kappa_j^2 = K^2 - \varepsilon_j\omega^2/c^2$, then changing amplitudes by bosonic operators through correspondence principle, they get the canonical form for electric field operator $\hat{\mathbf{E}} = \sum_k \left(\eta \mathbf{u}_k^{SPP}\hat{a} + c.c\right)$. They further claim single quantized excitation of any complex optical system generated by a single quanta source, either waveguide modes, or surface plasma wave, can be brought into this form, leaving spatial profile of the field (or pulse) invariant from classical normal mode function. To sum up, the literature claims

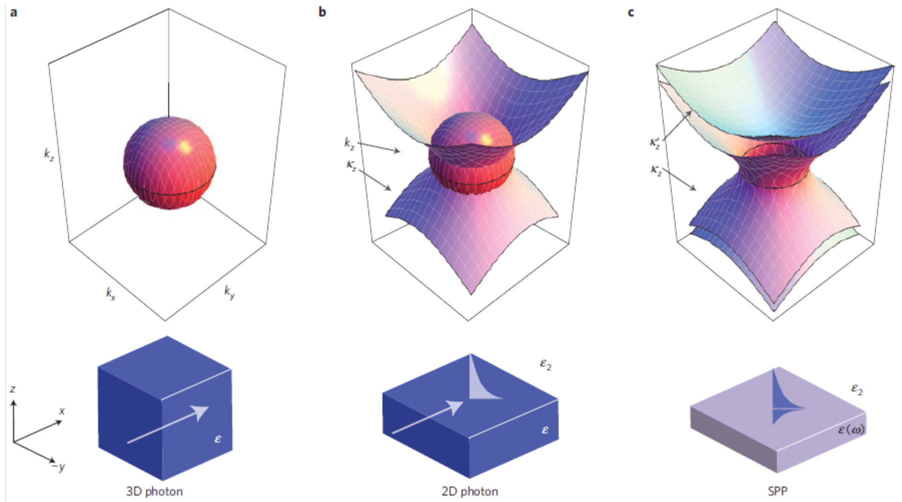

Figure 6.1: Spatial variance and dispersion relations of single photonic (polaritonic) excitations (adapted from Tame et al [15])

spatial information of single photons (polaritons), which are generated by processes like spontaneous emission, is carried by classical normal mode functions, and, the formalism of mode functions is equivalent to Green's tensors we use throughout this thesis. In the following subsections, we will test these claims by finding the pulse shapes generated by spontaneously emitting atoms on single dielectric layer, and inside l-HMM.

6.2 Spontaneously Emitted Pulse of an Atom On Single Dielectric Layer

To address the problem of finding the spatio-temporal distribution of the spontaneously emitted single photon pulse, Choquette et al [38] analyze the Heisenberg equations of motion in the second section. Their model assumes two level atom, which has electronic population Rabi oscillating between energy levels through transition dipoles, to be a quantum harmonic oscillator (or a quantum dipolar antenna) centered around transition frequency - by using smearing functions (Gaussian, double-Lorentzian etc). Initial state of the atom, an excited state, is given as,

$$|\psi_{init} >= \hat{b}_0|0 > \otimes|vac > \tag{6.10}$$

To get spontaneously emitted field, they use Laplace transformed, coupled Heisenberg equations shown in equations 3.96 and 3.97.

$$\begin{aligned}\mathbf{E}(\mathbf{r},s) &=< 0|\otimes < vac|\hat{\mathbf{E}}(\mathbf{r},s)0 > \otimes|vac > \\ &= \frac{i}{g}e_k\frac{\gamma_{ij}(\mathbf{r},s)+i\delta_{ij}(\mathbf{r},s)}{s+i\omega_0'+\gamma}\end{aligned} \tag{6.11}$$

When inverse Laplace transform is taken for the pole, $s = -i\omega_0' - \gamma$, and the identity $ImG_{ik} = (2i)^-1(G_{ik} - G_{ik}^*)$ is used, we end up with the following,

$$\mathbf{E}(\mathbf{r},t) = \frac{2g\hbar}{4\pi\epsilon_0}\hat{e}_k \cdot \int_0^\infty d\omega \frac{e^{-i\omega t}}{i(\omega_0-\omega)+\gamma}\frac{\omega^2}{c^2}G_{ik}(r,r_A;\omega,t) \tag{6.12}$$

Classical dipolar sources radiate the field, $\mathbf{E}(r) = \mathbf{G}(\mathbf{r}) \cdot \mu$, where μ is the dipole moment. Similarly, the integral above for quantum sources has its contributions coming from the pole (unless Green's dyad has other poles, but it does not have any other in our case), $\omega = \omega_0 - i\gamma$, making the field proportional to, $\mathbf{E} \propto \mu \cdot G_(r, r_A; \omega = \omega_0 - i\gamma, t)$.
The case we are interested in is an atom, whose transition dipole moment is in z direction, sitting on top of a planar interface, which spans xy directions. Atom is positioned at the origin, $\mathbf{r} = (0,0,0)$, the region above atom, $z > 0$ is filled with air, $n_1 = 1$, and the region below, $z < 0$, is flint-glass, $n_2 = \sqrt{\varepsilon_2} = 1.62$. Choquette et al [38] evaluate the above integral in far-field for Kreschmann configuration (air-metal-dielectric), $kr >> 1$.

The spatial Green's tensors of a dipole sitting on origin for layered dielectrics in far-field

[42] are given as follows,

$$\mathbf{G}_0(r) = \frac{e^{ikr}}{r}\begin{pmatrix} 1-\frac{x^2}{r^2} & -\frac{xy}{r^2} & -\frac{xz}{r^2} \\ -\frac{xy}{r^2} & 1-\frac{y^2}{r^2} & -\frac{yz}{r^2} \\ -\frac{xz}{r^2} & -\frac{yz}{r^2} & 1-\frac{z^2}{r^2} \end{pmatrix} \tag{6.13}$$

$$\mathbf{G}_{ref}(r) = \frac{e^{ikr}}{r}\begin{pmatrix} \frac{\Phi_1^{(3)}y^2}{\rho^2}+\frac{\Phi_1^{(2)}x^2z^2}{r^2\rho^2} & \frac{\Phi_1^{(2)}xyz^2}{r^2\rho^2}-\frac{\Phi_1^{(3)}xy}{\rho^2} & -\frac{\Phi_1^{(1)}xz}{r^2} \\ \frac{\Phi_1^{(2)}xyz^2}{r^2\rho^2}-\frac{\Phi_1^{(3)}xy}{\rho^2} & \frac{\Phi_1^{(3)}x^2}{\rho^2}+\frac{\Phi_1^{(2)}y^2z^2}{r^2\rho^2} & -\frac{\Phi_1^{(1)}yz}{r^2} \\ -\frac{\Phi_1^{(2)}xz}{r^2} & -\frac{\Phi_1^{(2)}yz}{r^2} & \Phi_1^{(1)}\left(1-\frac{z^2}{r^2}\right) \end{pmatrix} \tag{6.14}$$

$$\mathbf{G}_{tr}(r) = \frac{e^{ikn_2r}}{r}\begin{pmatrix} \frac{\Phi_n^{(3)}y^2}{\rho^2}+\frac{\Phi_n^{(2)}x^2z^2}{r^2\rho^2} & \frac{\Phi_n^{(2)}xyz^2}{r^2\rho^2}-\frac{\Phi_n^{(3)}xy}{\rho^2} & -\frac{\Phi_n^{(1)}xz}{r^2} \\ \frac{\Phi_n^{(2)}xyz^2}{r^2\rho^2}-\frac{\Phi_n^{(3)}xy}{\rho^2} & \frac{\Phi_n^{(3)}x^2}{\rho^2}+\frac{\Phi_n^{(2)}y^2z^2}{r^2\rho^2} & -\frac{\Phi_n^{(1)}yz}{r^2} \\ -\frac{\Phi_n^{(2)}xz}{r^2} & -\frac{\Phi_n^{(2)}yz}{r^2} & \Phi_n^{(1)}\left(1-\frac{z^2}{r^2}\right) \end{pmatrix} \tag{6.15}$$

Where the coefficients are functions of generalized Fresnel coefficients, in a bilayer system they are equivalent to usual Fresnel coefficients,

$$\begin{aligned} \Phi_1^{(1)} &= r^p \\ \Phi_1^{(2)} &= -r^p \\ \Phi_1^{(3)} &= r^s \\ \Phi_n^{(1)} &= t^p n_2 \frac{kn_2 z/r}{k_z} \\ \Phi_n^{(2)} &= -t^p n_2 \\ \Phi_n^{(3)} &= t^s \frac{kn_2 z/r}{k_z} \end{aligned} \tag{6.16}$$

Since classical field is given by dot-product of Green's tensor with dipole vector, $\mathbf{E} = \kappa_{coulomb}\mu\mathbf{G}\cdot\hat{\mu}$, for dipole pointing into z direction and $\kappa_{coulomb}\mu = \text{const}$, we have the following fields with implicit harmonic time dependence, $e^{-i\omega t}$,

$$E_x^{up,class} = -\frac{2\text{const}\varepsilon_2 w^3 xz\sqrt{\frac{z^2}{x^2+y^2+z^2}}e^{\frac{iw\sqrt{x^2+y^2+z^2}}{c}}}{c^2\left(x^2+y^2+z^2\right)^{3/2}\left(c\sqrt{\frac{w^2((\varepsilon_2-1)(x^2+y^2)+\varepsilon_2 z^2)}{c^2(x^2+y^2+z^2)}}+\varepsilon_2 w\sqrt{\frac{z^2}{x^2+y^2+z^2}}\right)} \tag{6.17}$$

$$E_y^{up,class} = -\frac{2\text{const}\varepsilon_2 w^3 yz\sqrt{\frac{z^2}{x^2+y^2+z^2}}e^{\frac{iw\sqrt{x^2+y^2+z^2}}{c}}}{c^2\left(x^2+y^2+z^2\right)^{3/2}\left(c\sqrt{\frac{w^2((\varepsilon_2-1)(x^2+y^2)+\varepsilon_2 z^2)}{c^2(x^2+y^2+z^2)}}+\varepsilon_2 w\sqrt{\frac{z^2}{x^2+y^2+z^2}}\right)} \tag{6.18}$$

$$E_z^{up,class} = \frac{2\text{const}\varepsilon_2 w^3\left(x^2+y^2\right)\sqrt{\frac{z^2}{x^2+y^2+z^2}}e^{\frac{iw\sqrt{x^2+y^2+z^2}}{c}}}{c^2\left(x^2+y^2+z^2\right)^{3/2}\left(c\sqrt{\frac{w^2((\varepsilon_2-1)(x^2+y^2)+\varepsilon_2 z^2)}{c^2(x^2+y^2+z^2)}}+\varepsilon_2 w\sqrt{\frac{z^2}{x^2+y^2+z^2}}\right)} \tag{6.19}$$

$$E_x^{down,class} = -\frac{2\text{const}\varepsilon_2 w^2 x\left(\frac{z^2}{x^2+y^2+z^2}\right)^{3/2}e^{\frac{i\sqrt{\varepsilon_2}w\sqrt{x^2+y^2+z^2}}{c}}\sqrt{\frac{w^2((\varepsilon_2-1)(x^2+y^2)+\varepsilon_2 z^2)}{c^2(x^2+y^2+z^2)}}}{cz^2\left(c\sqrt{\frac{w^2((\varepsilon_2-1)(x^2+y^2)+\varepsilon_2 z^2)}{c^2(x^2+y^2+z^2)}}+\varepsilon_2 w\sqrt{\frac{z^2}{x^2+y^2+z^2}}\right)} \tag{6.20}$$

$$E_y^{down,class} = -\frac{2\text{const}\varepsilon_2 w^2 y\left(\frac{z^2}{x^2+y^2+z^2}\right)^{3/2}e^{\frac{i\sqrt{\varepsilon_2}w\sqrt{x^2+y^2+z^2}}{c}}\sqrt{\frac{w^2((\varepsilon_2-1)(x^2+y^2)+\varepsilon_2 z^2)}{c^2(x^2+y^2+z^2)}}}{cz^2\left(c\sqrt{\frac{w^2((\varepsilon_2-1)(x^2+y^2)+\varepsilon_2 z^2)}{c^2(x^2+y^2+z^2)}}+\varepsilon_2 w\sqrt{\frac{z^2}{x^2+y^2+z^2}}\right)} \tag{6.21}$$

$$E_z^{down,class} = \frac{2\text{const}\varepsilon_2 w^2 z\left(x^2+y^2\right)e^{\frac{i\sqrt{\varepsilon_2}w\sqrt{x^2+y^2+z^2}}{c}}\sqrt{\frac{w^2((\varepsilon_2-1)(x^2+y^2)+\varepsilon_2 z^2)}{c^2(x^2+y^2+z^2)}}}{c\sqrt{\frac{z^2}{x^2+y^2+z^2}}\left(x^2+y^2+z^2\right)^2\left(c\sqrt{\frac{w^2((\varepsilon_2-1)(x^2+y^2)+\varepsilon_2 z^2)}{c^2(x^2+y^2+z^2)}}+\varepsilon_2 w\sqrt{\frac{z^2}{x^2+y^2+z^2}}\right)} \tag{6.22}$$

Using the Rubidium 87 D line data for the ground state transition $5^2S_{1/2} \to 5^2P_{3/2}$ [68], where $\omega_0 = 2\pi 384.230THz$, $\gamma = 2\pi 6.06MHz$, $\Omega_{Rabi} = 9.9KhZ$ and $\mu_{transition} = 4.22ea_0$, we have the following classical distribution of fields and intensity in bilayer dielectric stack and vacuum, and as we scale the electric fields in the graph by 1/const,

As seen in Fig 6.6, a classical dipole on vacuum pointing in z-direction emits non-directional light, two spherical bulges separated by the dipole vector, whose spatial information is carried out by $\mathbf{G}_0(r)$. When we add a second flint glass layer below $z = 0$ plane, the radiation generated by the dipole is transmitted/refracted to $z < 0$ and emit-

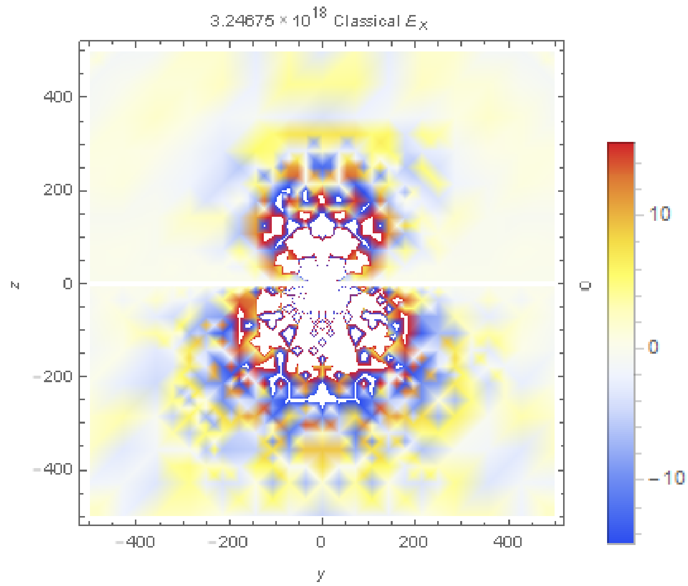

(a) (b)

Figure 6.2: Distribution of $E_x^{classical}$ in far-field, generated by a classical dipole on bilayer dielectric geometry.

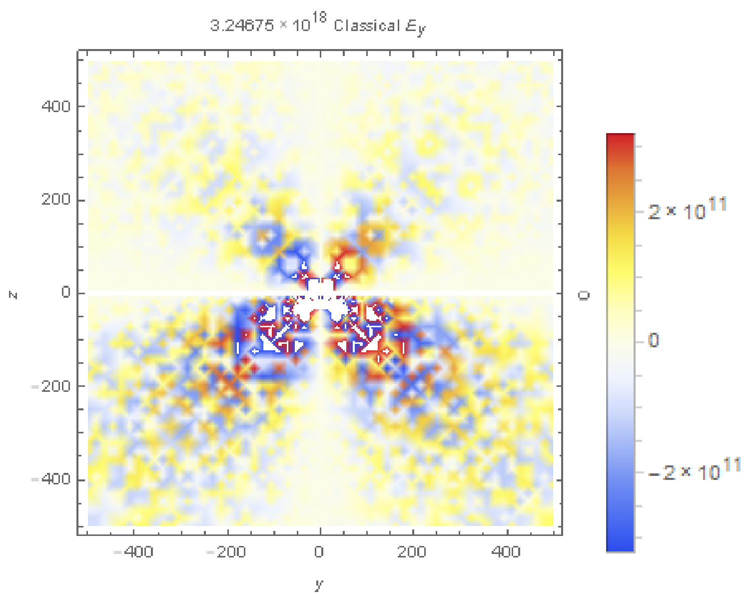

(a) (b)

Figure 6.3: Distribution of $E_y^{classical}$ in far-field, generated by a classical dipole on bilayer dielectric geometry.

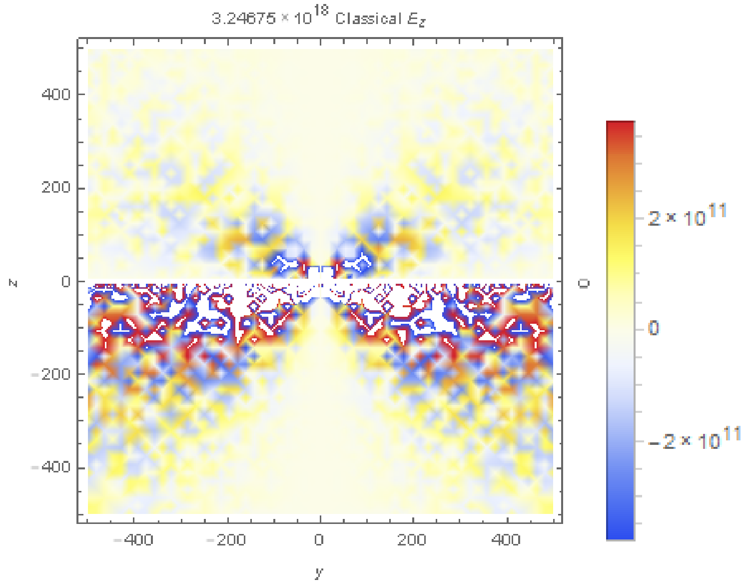

(a) (b)

Figure 6.4: Distribution of $E_z^{classical}$ in far-field, generated by a classical dipole on bilayer dielectric geometry.

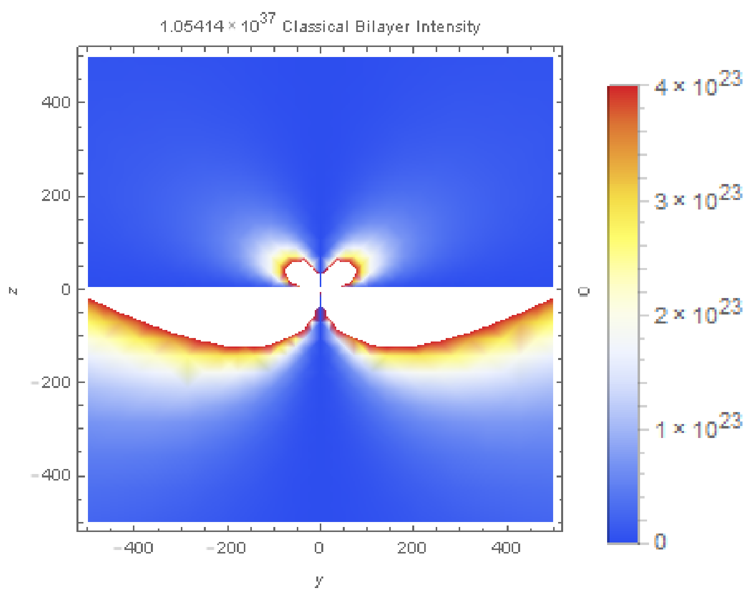

(a) (b)

Figure 6.5: Distribution of classical intensity, $I_{bilayer}^{classical}$ in far-field, generated by a classical dipole on bilayer dielectric geometry.

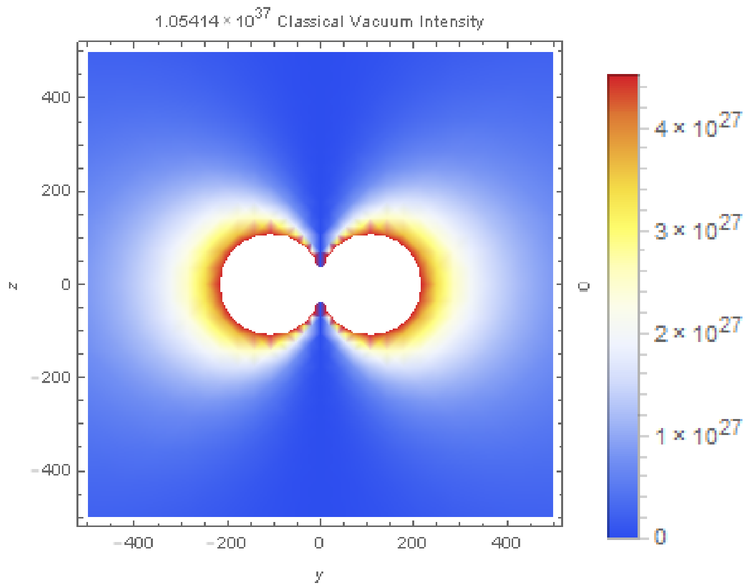

(a) (b)

Figure 6.6: Distribution of classical intensity, $I_{vacuum}^{classical}$ in far-field, generated by a classical dipole on vacuum.

ted/reflected to $z > 0$ as can be seen in Fig 6.2-6.5.

In the quantum case, where we have a spontaneously emitting atom (a quantum harmonic oscillator smeared out by a Gaussian centered by transition frequency ω_0, and Bohr-radius a_0 in our approximation) instead of a classical dipole, whose spatio-temporal field pattern (pulse shape) is given by Eq 6.12. In this equation, due to Lorentzian term in Fourier transform, we have all contributions coming from $\omega = \omega_0 - i\gamma$ pole, hence we get the spontaneously emitted single photon pulse shape on bilayer dielectric media as,

$$E_i^{quantum}(r,t) = \pi E_i^{classical}(r, \omega = \omega_0 - i\gamma)e^{-\gamma t}e^{-i\omega t} \tag{6.23}$$

By using Rubidium data [68], we get the following spatial field/intensity profiles,

Comparison of classical, Fig 6.2-6.6, and quantum, Fig 6.7-6.11, pulse shapes in spatial domain shows that they have same geometry. On the other hand, the $-i\gamma$ factor in the pole not only yields temporal decay by the term, $e^{-i\gamma t}$, but also making fields spatially

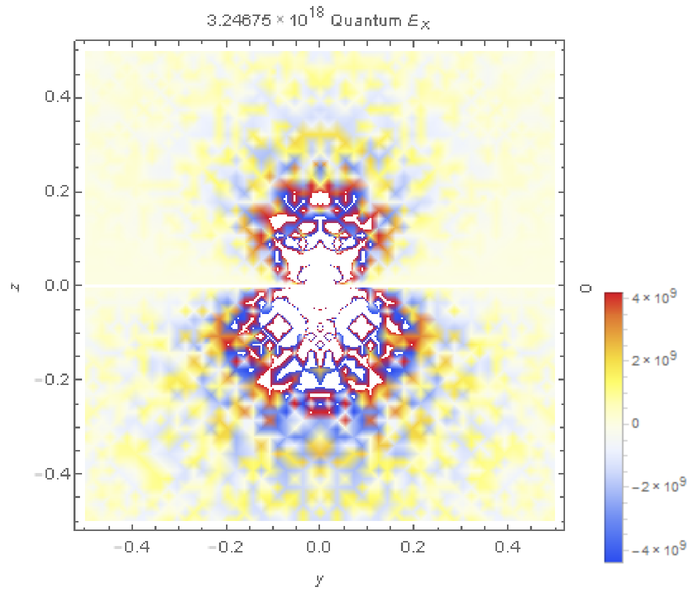

(a) (b)

Figure 6.7: Distribution of $E_x^{quantum}$ in far-field, generated by a spontaneously radiating atom on bilayer dielectric geometry.

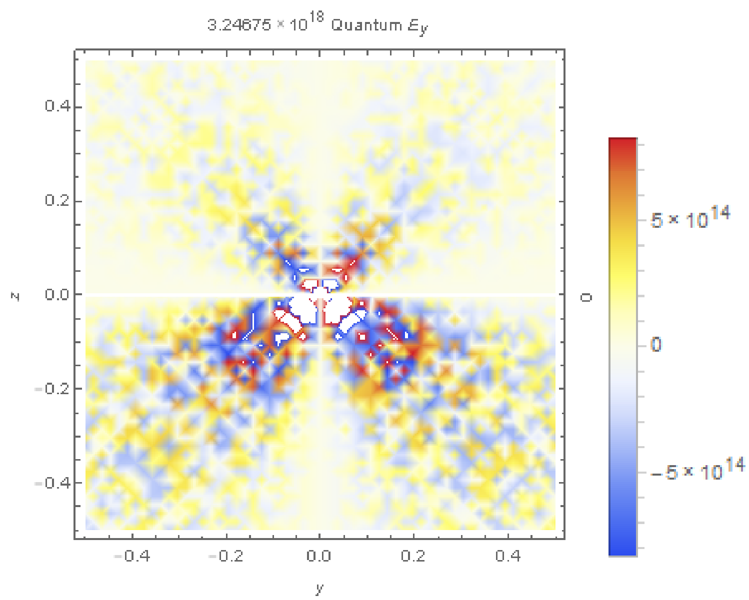

(a) (b)

Figure 6.8: Distribution of $E_y^{quantum}$ in far-field, generated by a a spontaneously radiating atom on bilayer dielectric geometry.

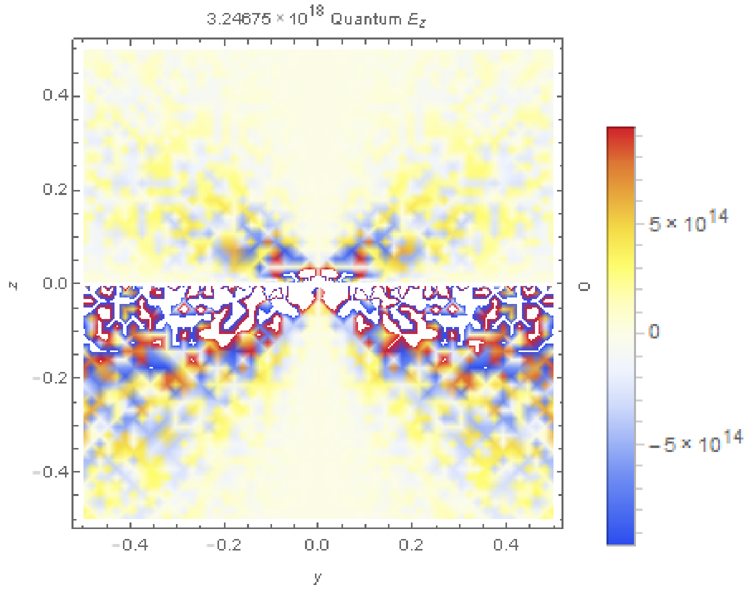

(a) (b)

Figure 6.9: Distribution of $E_z^{quantum}$ in far-field, generated by a spontaneously radiating atom on bilayer dielectric geometry.

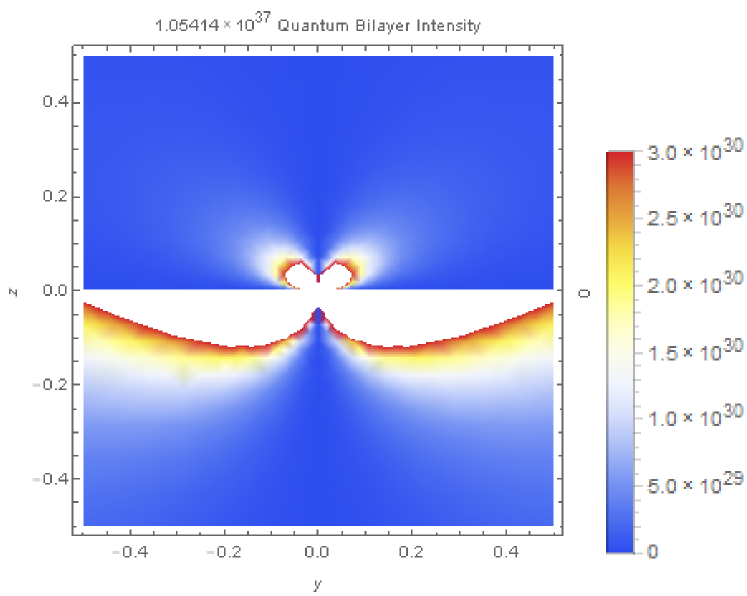

(a) (b)

Figure 6.10: Distribution of quantum intensity, $I_{bilayer}^{quantum}$ in far-field, generated by a spontaneously radiating atom on bilayer dielectric geometry.

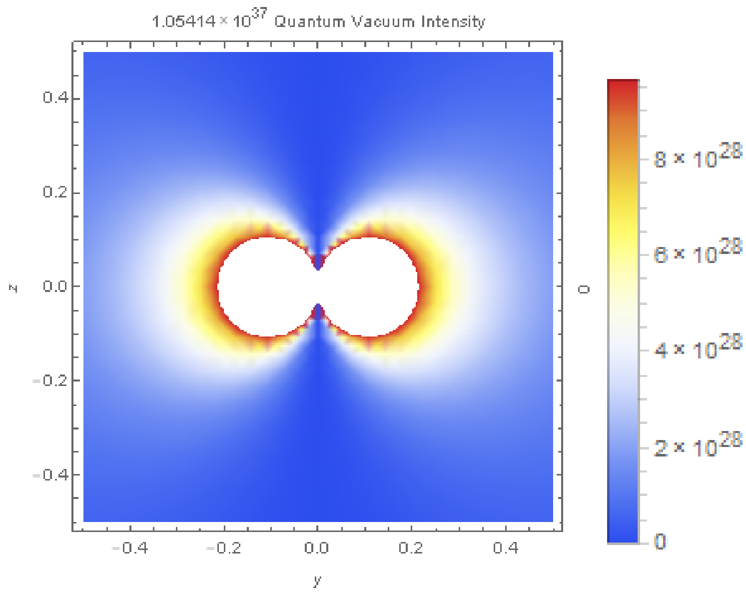

(a) (b)

Figure 6.11: Distribution of quantum intensity, $I^{quantum}_{vacuum}$ in far-field, generated by a spontaneously radiating atom on vacuum.

decaying faster, thus classical fields spread more than quantum ones by three orders of magnitude on graphs above.

6.3 Spontaneously Emitted Pulse inside l-HMM

For the pulse shape in l-HMM, we solve the equation, for Green's dyad given in equation 2.81.

$$\mathbf{E}(\mathbf{r},t) = \frac{2g\hbar}{4\pi\epsilon_0}\hat{e}_k \cdot \int_0^\infty d\omega \frac{e^{-i\omega t}}{i(\omega_0-\omega)+\gamma}\frac{\omega^2}{c^2}G_{ik}(r,r_A;\omega,t) \tag{6.24}$$

As shown by Potemkin et al [45], the singular part of Green's tensor does not affect field distribution other than atomic position, where singularity is, only affecting Purcell factor. Only contribution comes from the pole, $\omega = \omega_0 - i\gamma$, so we have the classical equation given by Potemkin [45] recovered, only by changing frequency with $\omega = \omega_0 - i\gamma$, leading to a decaying factor for harmonic time dependence. Since, according to Rubidium data [68] (and, for all atoms in general), transition frequency is six orders greater than decaying rate,

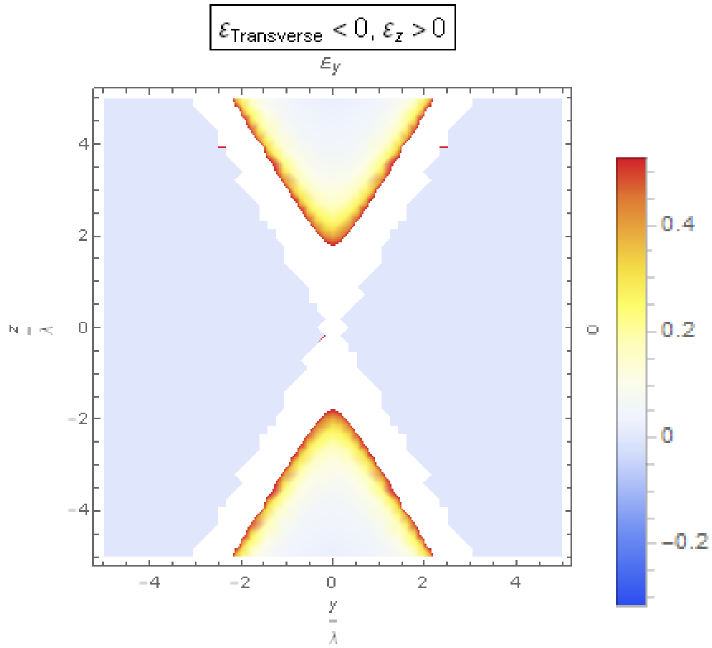

(a) (b)

Figure 6.12: Distribution of E_y in Type 1 l-Hmm, as the field scaled by λ^3/const

$\omega_0 >> \gamma$. For the THz orders of transition frequency, we have MHz, leaving the classical field distribution mostly unaffected.

Since the $g\hbar$ part of the formula brings $\Omega_{Rabi}\hbar/2$, and, hence $\mu E_0/2$, we scale our graphs by the dimensions of E_0 (usual pump laser strength in optics experiments), and by the orders of $\mu(1/4\pi\varepsilon_0)k^3$. We get the following graphs for $\lambda^3 E_i$,

Once we plot for the quantum case in Fig 6.12-6.15, we reproduce the pulse shapes given in Fig 2.12-2.15. For the type1 l-hmm we recover hourglass, and, for the type2 l-hmm we recover butterfly shape.

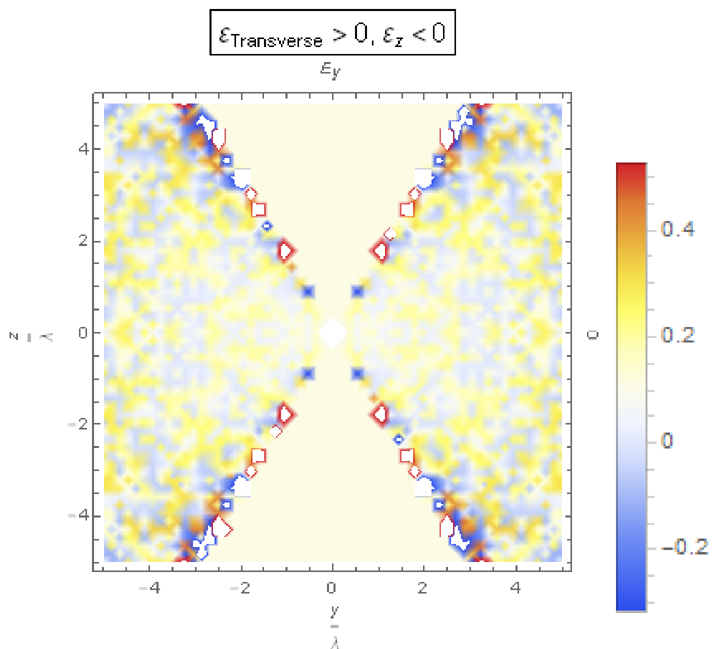

(a) (b)

Figure 6.13: Distribution of E_y in Type 2 l-Hmm, as the field scaled by λ^3/const

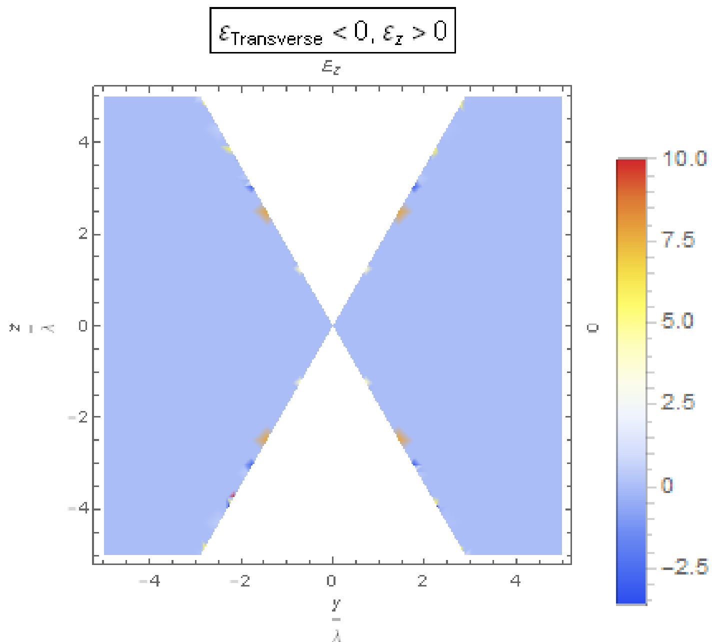

(a) (b)

Figure 6.14: Distribution of E_z in Type 1 l-Hmm, as the field scaled by λ^3/const. Please note that hourglass shape is recovered, and the white parts in color gradient are non-zero, but the blue parts are

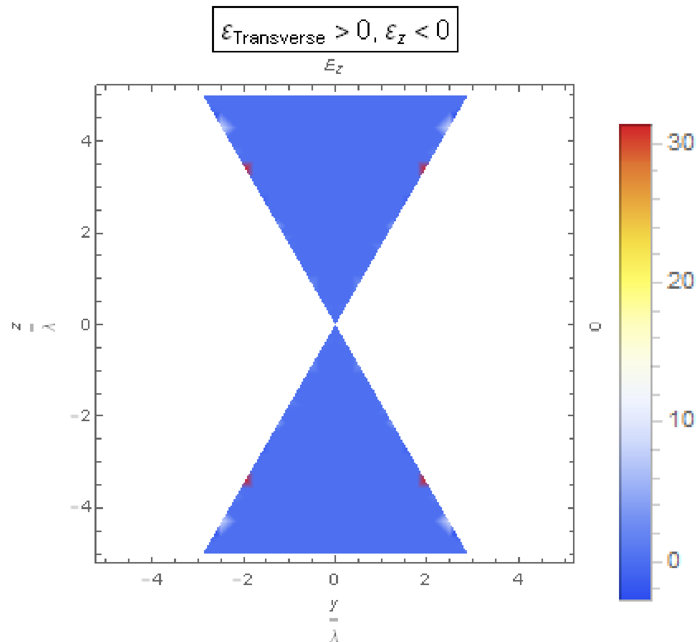

(a) (b)

Figure 6.15: Distribution of E_z in Type 2 l-Hmm, as the field scaled by λ^3/const. Please note that butterfly shape is recovered, and the white parts in color gradient are non-zero, but the blue parts are

BIBLIOGRAPHY

[1] D. P. DiVincenzo and IBM, "The physical implementation of quantum computation," *arXiv:quant-ph/0002077*, Feb. 2000. arXiv: quant-ph/0002077.

[2] J. I. Cirac, L. M. Duan, and P. Zoller, "Quantum optical implementation of quantum information processing," *arXiv:quant-ph/0405030*, May 2004. arXiv: quant-ph/0405030.

[3] C. Thiel, T. Bastin, J. Martin, E. Solano, J. von Zanthier, and G. S. Agarwal, "Quantum imaging with incoherent photons," *Physical Review Letters*, vol. 99, p. 133603, Sept. 2007.

[4] C. Thiel, T. Bastin, J. von Zanthier, and G. S. Agarwal, "Sub-rayleigh quantum imaging using single-photon sources," *Physical Review A*, vol. 80, p. 013820, July 2009.

[5] A. Kolkran and G. S. Agarwal, "Resolution of objects within subwavelength range by using the near field of a dipole," *Optics Letters*, vol. 37, p. 2313, June 2012.

[6] R. Wood, "Diffraction gratings with controlled groove form and abnormal distribution of intensity," *Philosophical magazine*, vol. 23, pp. 310–317, 1912.

[7] W. Wood, R. W, "On a remarkable case of uneven distribution of light in a diffraction grating spectrum," *Philysophical magazine*, vol. 4, pp. 396–402, 1902.

[8] L. Rayleigh, "Dynamical theory of the grating.," *Proc.Roy.Soc.(London)*, vol. A79, no. 399, 1907.

[9] N. Engheta and R. W. Ziolkowski, eds., *Metamaterials: Physics and Engineering Explorations*. Wiley-IEEE Press, Aug. 2006.

[10] A. Sommerfeld *Ann. Phys.*, vol. 28, p. 665, 1909.

[11] J. Zenneck *Ann. Phys.*, vol. 60, p. 481, 1919.

[12] H. Weyl *Ann. Phys.*, vol. 60, p. 481, 1919.

[13] U. Fano, "Atomic theory of electromagnetic interactions in dense materials," *Physical Review*, vol. 103, pp. 1202–1218, Sept. 1956.

[14] J. J. Hopfield, "Theory of the contribution of excitons to the complex dielectric constant of crystals," *Physical Review*, vol. 112, pp. 1555–1567, Dec. 1958.

[15] M. S. Tame, K. R. McEnery, . K. zdemir, J. Lee, S. A. Maier, and M. S. Kim, "Quantum plasmonics," *Nature Physics*, vol. 9, pp. 329–340, June 2013.

[16] D. E. Chang, A. S. Srensen, P. R. Hemmer, and M. D. Lukin, "Quantum optics with surface plasmons," *Physical Review Letters*, vol. 97, p. 053002, Aug. 2006.

[17] D. Martn-Cano, A. Gonzlez-Tudela, L. Martn-Moreno, F. J. Garca-Vidal, C. Tejedor, and E. Moreno, "Dissipation-driven generation of two-qubit entanglement mediated by plasmonic waveguides," *Physical Review B*, vol. 84, p. 235306, Dec. 2011.

[18] D. Dzsotjan, A. S. Srensen, and M. Fleischhauer, "Quantum emitters coupled to surface plasmons of a nanowire: A green's function approach," *Physical Review B*, vol. 82, p. 075427, Aug. 2010.

[19] E. Moreno, F. J. Garca-Vidal, D. Erni, J. I. Cirac, and L. Martn-Moreno, "Theory of plasmon-assisted transmission of entangled photons," *Physical Review Letters*, vol. 92, p. 236801, June 2004.

[20] A. Gonzalez-Tudela, P. A. Huidobro, L. Martin-Moreno, C. Tejedor, and F. J. Garcia-Vidal, "Theory of the strong coupling between quantum emitters and propagating surface plasmons," *Physical Review Letters*, vol. 110, Mar. 2013. arXiv: 1205.3938.

[21] T. Hmmer, F. J. Garca-Vidal, L. Martn-Moreno, and D. Zueco, "Weak and strong coupling regimes in plasmonic QED," *Physical Review B*, vol. 87, p. 115419, Mar. 2013.

[22] C. Gonzalez-Ballestero, E. Moreno, and F. J. Garcia-Vidal, "Generation, manipulation, and detection of two-qubit entanglement in waveguide QED," *Physical Review A*, vol. 89, Apr. 2014. arXiv: 1404.2749.

[23] J. Yang, G. W. Lin, Y. P. Niu, and S. Q. Gong, "Quantum entangling gates using the strong coupling between two optical emitters and nanowire surface plasmons," *Optics Express*, vol. 21, p. 15618, July 2013.

[24] J. B. Pendry, "Negative refraction makes a perfect lens," *Physical Review Letters*, vol. 85, pp. 3966–3969, Oct. 2000.

[25] D. Shin, Y. Urzhumov, Y. Jung, G. Kang, S. Baek, M. Choi, H. Park, K. Kim, and D. R. Smith, "Broadband electromagnetic cloaking with smart metamaterials," *Nature Communications*, vol. 3, p. 1213, Nov. 2012.

[26] A. Tuniz, K. J. Kaltenecker, B. M. Fischer, M. Walther, S. C. Fleming, A. Argyros, and B. T. Kuhlmey, "Metamaterial fibres for subdiffraction imaging and focusing at terahertz frequencies over optically long distances," *Nature Communications*, vol. 4, Oct. 2013.

[27] P. Shekhar, J. Atkinson, and Z. Jacob, "Hyperbolic metamaterials: fundamentals and applications," *Nano Convergence*, vol. 1, no. 1, p. 14, 2014. arXiv: 1401.2453.

[28] Z. Jacob. PhD thesis.

[29] V. P. Drachev, V. A. Podolskiy, and A. V. Kildishev, "Hyperbolic metamaterials: new physics behind a classical problem," *Optics Express*, vol. 21, p. 15048, June 2013.

[30] H. N. S. Krishnamoorthy, Z. Jacob, E. Narimanov, I. Kretzschmar, and V. M. Menon, "Topological transitions in metamaterials," *Science*, vol. 336, pp. 205–209, Apr. 2012.

[31] Z. Jacob, L. V. Alekseyev, and E. Narimanov, "Optical hyperlens: Far-field imaging beyond the diffraction limit," *Optics Express*, vol. 14, no. 18, p. 8247, 2006.

[32] Z. Liu, W. Li, and X. Jiang, "Controlling spontaneous emission of a two-level atom by hyperbolic metamaterials," *arXiv:1203.0618 [physics, physics:quant-ph]*, Mar. 2012. arXiv: 1203.0618.

[33] A. N. Poddubny, P. A. Belov, and Y. S. Kivshar, "Spontaneous radiation of a finite-size dipole emitter in hyperbolic media," *Physical Review A*, vol. 84, p. 023807, Aug. 2011.

[34] W. D. Newman, C. L. Cortes, and Z. Jacob, "Enhanced and directional single-photon emission in hyperbolic metamaterials," *Journal of the Optical Society of America B*, vol. 30, p. 766, Apr. 2013.

[35] C. L. Cortes, W. Newman, S. Molesky, and Z. Jacob, "Quantum nanophotonics using hyperbolic metamaterials," *Journal of Optics*, vol. 14, p. 063001, June 2012.

[36] S. A. Maier, *Plasmonics: Fundamentals and Applications* . Springer, 2007.

[37] L. Knoll, S. Scheel, and D.-G. Welsch, "QED in dispersing and absorbing media," *arXiv:quant-ph/0006121*, June 2000. arXiv: quant-ph/0006121.

[38] J. Choquette. PhD thesis.

[39] J. Weber, "Fluctuation dissipation theorem," *Physical Review*, vol. 101, pp. 1620–1626, Mar. 1956.

[40] R. D. L. Kronig, "ON THE THEORY OF DISPERSION OF x-RAYS," *Journal of the Optical Society of America*, vol. 12, p. 547, June 1926.

[41] P. B. Johnson and R. W. Christy, “Optical constants of the noble metals,” *Physical Review B*, vol. 6, pp. 4370–4379, Dec. 1972.

[42] L. Novotny, *Principles of Nano-Optics.* Cambridge University Press, 2012.

[43] V. M. Shalaev, ed.

[44] E. M. Purcell, H. C. Torrey, and R. V. Pound, “Resonance absorption by nuclear magnetic moments in a solid,” *Physical Review*, vol. 69, pp. 37–38, Jan. 1946.

[45] A. S. Potemkin, A. N. Poddubny, P. A. Belov, and Y. S. Kivshar, “Green function for hyperbolic media,” *Physical Review A*, vol. 86, p. 023848, Aug. 2012.

[46] A. Y. Nikitin, F. J. Garcia-Vidal, and L. Martin-Moreno, “Analytical expressions for the electromagnetic dyadic green’s function in graphene and thin layers,” *arXiv:1208.1397 [cond-mat]*, Aug. 2012. arXiv: 1208.1397.

[47] M. Paulus, P. Gay-Balmaz, and O. J. F. Martin, “Accurate and efficient computation of the green’s tensor for stratified media,” *Physical Review E*, vol. 62, pp. 5797–5807, Oct. 2000.

[48] R. W. Boyd and J. E. Sipe, “Nonlinear optical susceptibilities of layered composite materials,” *Journal of the Optical Society of America B*, vol. 11, p. 297, Feb. 1994.

[49] A. Salandrino and N. Engheta, “Far-field subdiffraction optical microscopy using metamaterial crystals: Theory and simulations,” *Physical Review B*, vol. 74, p. 075103, Aug. 2006.

[50] C. Guclu, S. Campione, and F. Capolino, “Hyperbolic metamaterial as super absorber for scattered fields generated at its surface,” *Physical Review B*, vol. 86, p. 205130, Nov. 2012.

[51] W. Weiglhofer, “Symbolic derivation of the electrodynamic greens tensor in an anisotropic medium,” *American Journal of Physics*, vol. 56, pp. 1095–1097, Dec. 1988.

[52] W. Weiglhofer, "Deltafunction identities and electromagnetic field singularities," *American Journal of Physics*, vol. 57, pp. 455–456, May 1989.

[53] H. C. Chen, *Theory of Electromagnetic Waves: A Coordinate-Free Approach.* Mcgraw Hill Series in Electrical and Computer Engineering, Mcgraw-Hill (Tx), Feb. 1983.

[54] A. Iyer, K. Balmain, and G. Eleftheriades, "Dispersion analysis of resonance cone behaviour in magnetically anisotropic transmission-line metamaterials," in *IEEE Antennas and Propagation Society International Symposium, 2004*, vol. 3, pp. 3147–3150 Vol.3, June 2004.

[55] O. Siddiqui and G. Eleftheriades, "Resonance-cone focusing in a compensating bilayer of continuous hyperbolic microstrip grids," *Applied Physics Letters*, vol. 85, pp. 1292–1294, Aug. 2004.

[56] K. Balmain, A. Luttgen, and P. Kremer, "Resonance cone formation, reflection, refraction, and focusing in a planar anisotropic metamaterial," *IEEE Antennas and Wireless Propagation Letters*, vol. 1, no. 1, pp. 146–149, 2002.

[57] C. K. Carniglia and L. Mandel, "Quantization of evanescent electromagnetic waves," *Physical Review D*, vol. 3, pp. 280–296, Jan. 1971.

[58] J. M. Vigoureux, L. D'Hooge, and D. Van Labeke, "Quantization of evanescent electromagnetic waves: Momentum of the electromagnetic field very close to a dielectric medium," *Physical Review A*, vol. 21, pp. 347–355, Jan. 1980.

[59] H. T. Dung, L. Knll, and D.-G. Welsch, "Resonant dipole-dipole interaction in the presence of dispersing and absorbing surroundings," *Physical Review A*, vol. 66, Dec. 2002. arXiv: quant-ph/0205056.

[60] C. Raabe, L. Knll, and D.-G. Welsch, "Three-dimensional casimir force between absorbing multilayer dielectrics," *Physical Review A*, vol. 68, Sept. 2003. arXiv: quant-ph/0212154.

[61] M. Amooshahi, “Canonical quantization of electromagnetic field in an anisotropic polarizable and magnetizable medium,” *Journal of Mathematical Physics*, vol. 50, p. 062301, June 2009.

[62] A. Archambault, F. Marquier, J.-J. Greffet, and C. Arnold, “Quantum theory of spontaneous and stimulated emission of surface plasmons,” *Physical Review B*, vol. 82, p. 035411, July 2010.

[63] B. Huttner and S. M. Barnett, “Quantization of the electromagnetic field in dielectrics,” *Physical Review A*, vol. 46, pp. 4306–4322, Oct. 1992.

[64] L. G. Suttorp and A. J. van Wonderen, “Fano diagonalization of a polariton model for an inhomogeneous absorptive dielectric,” *Europhysics Letters (EPL)*, vol. 67, pp. 766–772, Sept. 2004. arXiv: quant-ph/0408008.

[65] J. J. Choquette and K.-P. Marzlin, “Excitation of atoms by single-photon pulses in the presence of surface plasmons,” *Physical Review A*, vol. 85, p. 063841, June 2012.

[66] M. S. Tame, C. Lee, J. Lee, D. Ballester, M. Paternostro, A. V. Zayats, and M. S. Kim, “Single-photon excitation of surface plasmon polaritons,” *Physical Review Letters*, vol. 101, p. 190504, Nov. 2008.

[67] C. Guclu, S. Campione, and F. Capolino, “Array of dipoles near a hyperbolic metamaterial: Evanescent-to-propagating floquet wave transformation,” *Physical Review B*, vol. 89, p. 155128, Apr. 2014.

[68] D. A. Steck, “Rubidium 87 D Line Data, available online at http://steck.us/alkalidata (revision 2.0.1, 2 May 2008).” May 2008.